MULTISCALE MODEL. SIMUL.
Vol. 15, No. 1, pp. 274–308

A MODEL FOR RAYLEIGH–TAYLOR MIXING AND INTERFACE TURNOVER*

RAFAEL GRANERO-BELINCHÓN† AND STEVE SHKOLLER‡

Abstract. We first develop a new mathematical model for two-fluid interface motion, subjected to the Rayleigh–Taylor (RT) instability in two-dimensional fluid flow, which in its simplest form, is given by $h_{tt}(\alpha,t) = Ag\Lambda h - \frac{\sigma}{\rho^+ + \rho^-}\Lambda^3 h - A\boldsymbol{p}_\alpha(Hh_t h_t)$, where $\Lambda = H\boldsymbol{p}_\alpha$ and H denotes the Hilbert transform. In this so-called h-model, A is the Atwood number, g is the acceleration, σ is surface tension, and $\rho^\pm$ denotes the densities of the two fluids. We derive our h-model using asymptotic expansions in the Birkhoff–Rott integral-kernel formulation for the evolution of an interface separating two incompressible and irrotational fluids. The resulting h-model equation is shown to be locally and globally well-posed in Sobolev spaces when a certain *stability condition* is satisfied; this stability condition requires that the product of the Atwood number and the initial velocity field be positive. The asymptotic behavior of these global solutions, as $t \to \infty$, is also described. The h-model equation is shown to have interesting balance laws, which distinguish the stable dynamics from the unstable dynamics. Numerical simulations of the h-model show that the interface can quickly grow due to nonlinearity, and then stabilize when the lighter fluid is on top of the heavier fluid and acceleration is directed downward. In the unstable case of a heavier fluid being supported by the lighter fluid, we find good agreement for the growth of the mixing layer with experimental data in the "rocket rig" experiment of Read and Youngs. We then derive an interface model for RT instability, with a general parameterization $z(\alpha,t) = (z_1(\alpha,t), z_2(\alpha,t))$ such that z satisfies $z_{tt} = \Lambda[\frac{A}{|\partial_\alpha z|^2}H(z_t\cdot(\partial_\alpha z)^\perp H(z_t\cdot(\partial_\alpha z)^\perp)) + \frac{[p]}{\rho^+ + \rho^-} + Agz_2]\frac{(\partial_\alpha z)^\perp}{|\partial_\alpha z|^2} + z_t\cdot(\partial_\alpha z)^\perp(\frac{(\partial_\alpha z_t)^\perp}{|\partial_\alpha z|^2} - \frac{(\partial_\alpha z)^\perp 2(\partial_\alpha z\cdot\partial_\alpha z_t)}{|\partial_\alpha z|^4})$. This more general RT z-model allows for interface turnover. Numerical simulations of the z-model show an even better agreement with the predicted mixing layer growth for the rocket rig experiment.

Key words. Rayleigh–Taylor instability, interface motion, interface growth rates, mixing, Kelvin–Helmholtz

AMS subject classifications. 76E17, 76F25, 35Q35, 35B35

DOI. 10.1137/16M1083463

1. Introduction.

The instability of a heavy fluid layer supported by a light one is generally known as Rayleigh–Taylor (RT) instability (see Rayleigh [12] and Taylor [17]). It can occur under gravity and, equivalently, under an acceleration of the fluid system in the direction toward the denser fluid; in particular, RT is an interface fingering instability, which occurs when a perturbed interface, between two fluids of different density, is subjected to a normal pressure gradient. Whenever the pressure is higher in the lighter fluid, the differential acceleration causes the two fluids to mix. See Sharp [16], Youngs [18, 19], and Kull [11] for an overview of the RT instability.

*Received by the editors July 6, 2016; accepted for publication (in revised form) December 1, 2016; published electronically February 22, 2017.

http://www.siam.org/journals/mms/15-1/M108346.html

Funding: The first author was supported by the LABEX MILYON (ANR-10-LABX-0070) of Université de Lyon, within the program "Investissements d'Avenir" (ANR-11-IDEX-0007) operated by the French National Research Agency (ANR) and by grant MTM2014-59488P from the Ministerio de Economia y Competitividad (MINECO, Spain). The second author was supported by the National Science Foundation grant DMS-1301380, and by the Department of Energy Advanced Simulation and Computing (ASC) Program.

†Univ Lyon, Université Claude Bernard Lyon 1, CNRS UMR 5208, Institut Camille Jordan, 43 blvd. du 11 novembre 1918, F-69622 Villeurbanne cedex, France (granero@math.univ-lyon1.fr).

‡Department of Mathematics, University of California, Davis, CA 95616 (shkoller@math.ucdavis.edu).

The Euler equations of inviscid hydrodynamics serve as the basic mathematical model for RT instability and mixing between two fluids. This highly unstable system of conservation laws is both difficult to analyze (as it is ill-posed in the absence of surface tension and viscosity) and difficult to computationally simulate at the small spatial scales of RT mixing. As such, our objective is to develop *model equations*, which can be used to predict the RT mixing layer and growth rate.

In order to derive our RT interface models, we shall assume both incompressible and irrotational flow for the two-fluid Euler equations. Rather than proceeding with a direct approximation of the Euler equations, we shall instead work with the equivalent Birkhoff–Rott singular integral-kernel formulation for the evolution of the material interface. We have found that this formulation possesses a certain robustness in regards to approximations founded upon expansions in various parameters.

In the simplest case, in which the interface is modeled as a graph $(\alpha, h(\alpha,t))$ of a signed *height* function $h(\alpha,t)$, our approach yields a second-order–in-time quadratically nonlinear wave equation for the position of the interface, the h-model, which is given by

$$h_{tt}(\alpha,t) = Ag\,\Lambda h - \frac{\sigma}{\rho^+ + \rho^-}\Lambda^3 h - A\partial_\alpha(Hh_t h_t)\,,$$

where $\Lambda = H\partial_\alpha$ and H denotes the Hilbert transform. In this h-model equation, A denotes the Atwood number, g is the acceleration, $\sigma \geq 0$ is the surface tension, and $\rho^\pm > 0$ denotes the densities of the two fluids.

As we will describe below, our h-model equation for RT instability is both locally and globally well-posed in Sobolev spaces when a stability condition is satisfied, which requires the product of the Atwood number and the initial velocity field to be positive. Under such a stability condition, we also derive the asymptotic behavior of solutions to the h-model as $t \to \infty$. A number of interesting energy laws are also derived, which distinguish between stable and unstable interface dynamics

Numerical simulations are performed, which show that the h-model is capable of producing remarkable growth of the interface, followed by (possibly oscillatory) decay to a rest state in the case that the lighter fluid is supported by the heavier fluid. In the highly unstable case, where a heavy fluid is supported by the lighter fluid, we perform the classical "rocket rig" experiment of Read [13] and Youngs [19] for the case of unstable RT mixing layer growth, and find very good agreement for the growth rates with the predicted quadratic growth rate of Youngs [19], and with both direct numerical simulations (DNS) and experimental data.

Finally, in order to allow for the interface to turn over (rather than simply remaining a graph) we develop a more general z-model for the interface parameterization $z(\alpha,t) = (z_1(\alpha,t), z_2(\alpha,t))$ which satisfies

$$\begin{aligned} z_{tt} = \Lambda\left[\frac{A}{|\partial_\alpha z|^2} H\left(z_t\cdot(\partial_\alpha z)^\perp H(z_t\cdot(\partial_\alpha z)^\perp)\right) + \frac{[\![p]\!]}{\rho^+ + \rho^-} + Agz_2\right]\frac{(\partial_\alpha z)^\perp}{|\partial_\alpha z|^2} \\ + z_t\cdot(\partial_\alpha z)^\perp\left(\frac{(\partial_\alpha z_t)^\perp}{|\partial_\alpha z|^2} - \frac{(\partial_\alpha z)^\perp 2(\partial_\alpha z\cdot\partial_\alpha z_t)}{|\partial_\alpha z|^4}\right). \end{aligned}$$

Rather than constraining the interface amplitude to grow at the RT instability, the z-model can allow for interface turnover. We perform numerical simulations to demonstrate the improvement afforded by this more general model, and the even better accuracy in matching the predicted growth of the RT mixing layer for the rocket rig experiment. We also perform the so-called "tilted rig" experiment, in which the tank holding the fluid is tilted by a small angle away from vertical. Again,

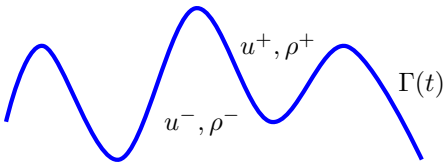

FIG. 1. *The blue curve is an illustration of the interface* $\Gamma(t)$*, separating two fluids at a time* $t \in [0,T]$*. The fluid on top of* $\Gamma(t)$ *has density* ρ^+*, while the fluid on the bottom has density* ρ^-*.*

our simulations demonstrate good qualitative agreement with DNS. To conclude, we also perform a numerical simulation for a Kelvin–Helmholtz problem, for which the Atwood number is set to zero to prevent an RT instability; starting from a steep mode-1 wave, we show roll-over of the interface with a very localized energy spectrum.

2. Equations for multiphase flow. The Euler equations are a system of conservation laws, modeling the dynamics of multiphase inviscid fluid flow. For incompressible two-dimensional motion, the conservation of momentum for a homogeneous, inviscid fluid can be written as

$$\rho\big(u_t + (u\cdot\nabla)u\big) + \nabla p = -g\rho e_2, \tag{1}$$

where $u = (u_1, u_2)$ denotes the velocity vector field of the fluid, p is the scalar pressure function, ρ is the density, g is the acceleration, $\nabla = (\partial_{x_1}, \partial_{x_2})$ is the gradient vector, and $e_2 = (0,1)$.

For incompressible flow, the conservation of mass is given by

$$\nabla \cdot u = 0\,.$$

We shall further assume that the fluid is irrotational so that

$$\omega := \operatorname{curl} u = 0, \tag{2}$$

where ω is the vorticity of the fluid, and $\operatorname{curl} u = \partial_1 u^2 - \partial_2 u^1$.

We assume that there are two fluids with densities ρ^+ and ρ^-, separated by a material interface $\Gamma(t)$, where t denotes an instant of time in the interval $[0,T]$. As shown in Figure 1, the fluid with density ρ^+ lies above $\Gamma(t)$, while the fluid with density ρ^- lies below $\Gamma(t)$.

For each instant of time $t \in [0,T]$, the interface $\Gamma(t)$ is parameterized by a function $z(\alpha,t)$. We will provide a special choice for the parameterization $z(\alpha,t)$ below.

We denote the jump of a field variable $f(x,t)$ across $\Gamma(t)$ by

$$[\![f]\!] = f^+ - f^-\,.$$

We let n and τ denote the unit normal and tangent vectors to $\Gamma(t)$, respectively; for the RT instability, we have the following jump conditions:

$$[\![u\cdot n]\!] = 0\,, \quad [\![u\cdot\tau]\!] \neq 0 \quad \text{on } \Gamma(t)\,. \tag{3}$$

Note that $\partial_\alpha z(\alpha,t)$ is a tangent vector to $\Gamma(t)$ at the point $z(\alpha,t)$, so that

$$[\![u\cdot\partial_\alpha z]\!] \neq 0.$$

Consequently, the velocity is not continuous at the interface. Due to the fact that the *shape* of the interface is determined only by the normal component of the fluid velocity, the motion of the interface has a tangential reparameterization symmetry, so that we can add any tangential velocity to the motion of the interface, with the hope that this will simplify the analysis. As such, the evolution equation for the parameterization of $\Gamma(t)$ is written as

$$z_t(\alpha,t) = u(z(\alpha,t),t) + c(\alpha,t)\partial_\alpha z(\alpha,t), \tag{4}$$

where the function $c(\alpha,t)$ will be specified below.

3. The integral kernel formulation. A number of modal models have been proposed for the evolution of the RT mixing layer; see, for example, Rollin and Andrews [15] and Goncharov [8], and the references therein. These modal models are based on a modal decomposition and approximation of the evolution equations for the parameterization of the interface and the velocity potential; such models consist of a large coupled system of nonlinear ODEs for a finite set of Fourier modes.

Rather than developing a modal model for RT mixing and approximating the partial differential equations themselves, we shall take another approach to the development of an RT model, which is founded upon the Birkhoff–Rott integral-kernel formulation for the evolution of an interface, separating two incompressible and irrotational fluids.

In order to introduce the integral-kernel formulation, which consists of *singular integrals*, we begin by defining the *principal value integral* of a given function f as

$$\text{P.V.} \int_{\mathbb{R}} f(\beta)d\beta = \lim_{\epsilon\to 0^+} \int_{(-1/\epsilon,-\epsilon)\cup(\epsilon,1/\epsilon)} f(\beta)d\beta\,.$$

The well-known Biot–Savart kernel $\mathcal{K}_{\text{BS}}$ is an integral representation for $\nabla^\perp\Delta^{-1}$, where $\nabla^\perp = (-\partial_{x_2},\partial_{x_1})$, and $\Delta = \partial_{x_1}^2 + \partial_{x_2}^2$ denotes the Laplace operator in the plane. In other words, if the two fluids fill the plane, then Δ^{-1} is given by the Newtonian potential and the Biot–Savart kernel is given by

$$\begin{aligned}\mathcal{K}_{\text{BS}}(x,y) &= \frac{1}{2\pi}\nabla^\perp \log(x)\\ &= \frac{1}{2\pi}\left(-\frac{x_2-y_2}{(x_2-y_2)^2+(x_1-x_1)^2}, \frac{x_1-y_1}{(x_2-y_2)^2+(x_1-y_1)^2}\right).\end{aligned} \tag{5}$$

Similarly, if the fluid flow is periodic in the horizontal variable, then

$$\mathcal{K}_{\text{BS}}(x,y) = \frac{1}{4\pi}\left(\frac{-\sinh(x_2-y_2)}{\cosh(x_2-y_2)-\cos(x_1-y_1)}, \frac{\sin(x_1-y_1)}{\cosh(x_2-y_2)-\cos(x_1-y_1)}\right). \tag{6}$$

Due to the characteristics of the irrotational flow, the *vorticity* is a measure which is supported on the interface $\Gamma(t)$, written as

$$\omega = \varpi\delta_{\Gamma(t)}\,,$$

where $\delta_{\Gamma(t)}$ is the Dirac delta function supported on the interface $\Gamma(t)$. More precisely, the vorticity ω is a distribution defined as follows: for all smooth test functions φ with compact support,

$$\omega(\varphi) = \int_{\mathbb{R}} \varpi(\beta,t)\varphi(z(\beta,t))d\beta\,.$$

The function ϖ is the *amplitude of the vorticity* along $\Gamma(t)$. Notice that ϖ is minus the jump of the velocity in the tangential direction:

$$\varpi = -[\![u \cdot \partial_\alpha z]\!].$$

Given the vorticity measure ϖ, we can reconstruct the velocity field everywhere; specifically, we have, thanks to the Biot–Savart law, that

$$u(x,t) = \text{P.V.} \int_{\mathbb{R}} \varpi(\beta) \mathcal{K}_{\text{BS}}(x, z(\beta,t)) d\beta. \tag{7}$$

Now, using the parameterization $z(\alpha,t)$ for the interface $\Gamma(t)$, we define the Birkhoff–Rott principal-value integral, denoting $\int_{\mathbb{R}}$ by $\int$, as

$$\mathcal{K}_{\text{BR}}(\alpha,t) = \text{P.V.} \int \varpi(\beta,t) \mathcal{K}_{\text{BS}}(z(\alpha), z(\beta,t)) d\beta. \tag{8}$$

In particular, (8) is explicitly given by

$$\mathcal{K}_{\text{BR}}(\alpha,t) = \frac{1}{2\pi} \text{P.V.} \int \varpi(\beta) \left(-\frac{z_2(\alpha,t) - z_2(\beta,t)}{|z(\alpha,t) - z(\beta,t)|^2}, \frac{z_1(\alpha,t) - z_1(\beta,t)}{|z(\alpha,t) - z(\beta,t)|^2} \right) d\beta. \tag{9}$$

The Birkhoff–Rott function $\mathcal{K}_{\text{BR}}(\alpha,t)$ denotes the average velocity at a given point $\alpha \in \Gamma(t)$, so that

$$\mathcal{K}_{\text{BR}} = \frac{u^+ + u^-}{2} \text{ on the interface } z(\alpha,t).$$

4. Dynamics of the interface and vorticity amplitude. We now formulate the dynamics of the interface. Since $z_t = u + c\partial_\alpha z$, we see that

$$z_t(\alpha,t) = \frac{1}{2\pi} P.V. \int \varpi(\beta) \frac{(z(\alpha,t) - z(\beta,t))^\perp}{|z(\alpha,t) - z(\beta,t)|^2} d\beta + c(\alpha,t) \partial_\alpha z(\alpha,t)\,. \tag{10}$$

A lengthy computation then shows [6] that

$$\begin{aligned} \varpi_t = -\partial_\alpha \Bigg[& \frac{A}{4\pi^2} \left| \int \varpi(\beta) \frac{(z(\alpha,t) - z(\beta,t))^\perp}{|z(\alpha,t) - z(\beta,t)|^2} d\beta \right|^2 - \frac{A}{4} \frac{\varpi(\alpha,t)^2}{|\partial_\alpha z(\alpha,t)|^2} \\ & + \frac{A}{\pi} \int \varpi(\beta) \frac{(z(\alpha,t) - z(\beta,t))^\perp}{|z(\alpha,t) - z(\beta,t)|^2} \cdot \partial_\alpha z(\alpha,t) c(\alpha,t) d\beta \\ & - c(\alpha,t)\varpi(\alpha,t) - \frac{2[\![p]\!]}{\rho^+ + \rho^-} - 2Agz_2 \Bigg] \\ & + \frac{A}{\pi} \partial_t \left[\int \varpi(\beta) \frac{(z(\alpha,t) - z(\beta,t))^\perp}{|z(\alpha,t) - z(\beta,t)|^2} \cdot \partial_\alpha z(\alpha,t) d\beta \right]. \end{aligned} \tag{11}$$

5. The case that the interface $\Gamma(t)$ is a graph. We now assume that the interface $\Gamma(t)$ is the graph of the signed height function $h(\alpha,t)$, so that the parameterization $z(\alpha,t)$ is given by

$$(z_1(\alpha,t), z_2(\alpha,t)) = (\alpha, h(\alpha,t))\ . \tag{12}$$

If at time $t = 0$, $\Gamma(0)$ is given as the graph $(\alpha, h(\alpha,0))$, then we can ensure that $\Gamma(t)$ stays a graph for future time $t > 0$ by making an explicit choice of the function $c(\alpha,t)$ in (4). To this end, we define

$$c(\alpha,t) = \frac{1}{2\pi} P.V. \int \varpi(\beta) \frac{h(\alpha,t) - h(\beta,t)}{(\alpha-\beta)^2 + (h(\alpha,t) - h(\beta,t))^2} d\beta\,. \tag{13}$$

With $\Gamma(t)$ given by $(\alpha, h(\alpha,t))$, the definition of the Birkhoff–Rott function $\mathcal{K}_{\mathrm{BR}}(\alpha,t)$ in (8) simplifies to

(14)
$$\mathcal{K}_{\mathrm{BR}}(\alpha,t)(\alpha,t) = \frac{1}{2\pi} P.V. \int \frac{\varpi(\beta,t)}{\alpha-\beta} \left(\frac{-\frac{h(\alpha,t)-h(\beta,t)}{\alpha-\beta}}{1+\left(\frac{h(\alpha,t)-h(\beta,t)}{\alpha-\beta}\right)^2}, \frac{1}{1+\left(\frac{h(\alpha,t)-h(\beta,t)}{\alpha-\beta}\right)^2} \right),$$

the evolution equation for $\Gamma(t)$ can be written in terms of the height function $h(\alpha,t)$ as

$$h_t(\alpha,t) = \frac{1}{2\pi} P.V. \int \frac{\varpi(\beta,t)}{\alpha-\beta} \frac{1}{1+\left(\frac{h(\alpha,t)-h(\beta,t)}{\alpha-\beta}\right)^2} d\beta + c(\alpha,t)\partial_\alpha h(\alpha,t), \tag{15}$$

and the evolution equation for vorticity ϖ on $\Gamma(t)$ takes the form

$$\begin{aligned} \varpi_t(\alpha,t) = {} & \frac{A}{4}\partial_\alpha \left(\frac{\varpi^2(\alpha,t)}{1+(\partial_\alpha h(\alpha,t))^2} \right) + \partial_\alpha(c(\alpha,t)\varpi(\alpha,t)) + \frac{2}{\rho^+ + \rho^-}\partial_\alpha [\![p]\!] \\ & + 2A\partial_\alpha \mathcal{K}_{\mathrm{BR}}(\alpha,t)\cdot(1,\partial_\alpha h)c(\alpha,t) + 2Ag\partial_\alpha h + 2A\partial_t \mathcal{K}_{\mathrm{BR}}(\alpha,t)\cdot(1,\partial_\alpha h). \end{aligned} \tag{16}$$

6. A simple model equation for RT instability. In this section, we shall derive a model of RT instability in which the interface $\Gamma(t)$ is a graph of the height function $h(\alpha,t)$. In order to proceed with our derivation, we shall make further approximations to the coupled system of (15) and (16).

6.1. The equations in the linear regime. In the linear regime, (15) and (16) reduce to the following coupled system:

$$h_t(\alpha,t) = \frac{1}{2} H\varpi, \tag{17a}$$

$$\varpi_t(\alpha,t) = +2Ag\partial_\alpha h + \frac{2\sigma}{\rho^+ + \rho^-}\partial_\alpha^3 h, \tag{17b}$$

where H denotes the Hilbert transform, defined as

$$H\varpi(\alpha) = \frac{1}{\pi} P.V. \int \frac{\varpi(\beta)}{\alpha-\beta} d\beta. \tag{18}$$

6.2. The nonlinear regime and the model equation. Having found the linear dynamics, we turn our attention to the the nonlinear regime. Our objective is to derive a model equation which contains the quadratic nonlinearities. To do so, we shall introduce some further notation.

We define the operator Λ by

$$\Lambda\varpi = H\partial_\alpha \varpi,$$

and the space-integrated vorticity as

$$\langle\varpi\rangle(t) = \int \varpi(\beta,t) d\beta.$$

We shall use the notation $\langle f\rangle(t)$ to denote $\int f(\beta,t)d\beta$ for any integrable function $f(\beta,t)$.

We make use of the following power series expansions for $|\zeta| < 1$:

$$\frac{1}{1+\zeta^2} = 1 - \zeta^2 + \zeta^4 - \zeta^6 + \cdots,$$

and

$$\frac{\zeta}{1+\zeta^2} = \zeta - \zeta^3 + \zeta^5 - \zeta^7 + \cdots.$$

Using these identities together with the approximation

$$\frac{h(\alpha) - h(\beta)}{\alpha - \beta} \approx \partial_\alpha h(\alpha) + \frac{1}{2}\partial_\alpha^2 h(\alpha)(\beta - \alpha),$$

the nonlocal terms in (15) and (16) can be approximated as

$$\begin{aligned}
c(\alpha,t)\partial_\alpha h(\alpha,t) &\approx \frac{\partial_\alpha h(\alpha,t)}{2\pi} P.V. \int \frac{\varpi(\beta)}{\alpha-\beta} \frac{h(\alpha,t)-h(\beta,t)}{\alpha-\beta} d\beta\,,\\
\mathcal{K}_{\mathrm{BR}}(\alpha,t) &\approx \frac{1}{2\pi} P.V. \int \frac{\varpi(\beta,t)}{\alpha-\beta} \left(-\frac{h(\alpha,t)-h(\beta,t)}{\alpha-\beta}\,, \right.\\
&\qquad \left. 1 - \left(\frac{h(\alpha,t)-h(\beta,t)}{\alpha-\beta} \right)^2 \right),\\
\partial_\alpha \mathcal{K}_{\mathrm{BR}}(\alpha,t)\cdot(1,\partial_\alpha h) c(\alpha,t) &\approx -\frac{1}{2}\partial_\alpha \left(\frac{1}{2\pi} P.V. \int \frac{\varpi(\beta)}{\alpha-\beta} \frac{h(\alpha,t)-h(\beta,t)}{\alpha-\beta} d\beta \right)^2\\
&\quad + \frac{1}{2}\Lambda\varpi\partial_\alpha h \frac{1}{2\pi} P.V. \int \frac{\varpi(\beta)}{\alpha-\beta} \frac{h(\alpha,t)-h(\beta,t)}{\alpha-\beta} d\beta\\
&\approx -\frac{1}{2}\partial_\alpha \left(\frac{\partial_\alpha h}{2} H\varpi - \frac{\partial_\alpha^2 h}{4\pi}\langle\varpi\rangle \right)^2\\
&\quad + \frac{1}{2}\Lambda\varpi\partial_\alpha h \left(\frac{\partial_\alpha h}{2} H\varpi - \frac{\partial_\alpha^2 h}{4\pi}\langle\varpi\rangle \right),
\end{aligned}$$

and

$$\begin{aligned}
\partial_t \mathcal{K}_{\mathrm{BR}}(\alpha,t)\cdot(1,\partial_\alpha h) &\approx \frac{1}{2\pi} P.V. \int \frac{\varpi_t(\beta)}{\alpha-\beta} \left(-\frac{h(\alpha,t)-h(\beta,t)}{\alpha-\beta} + \partial_\alpha h(\alpha) \right) d\beta\\
&\quad - \frac{1}{2} H\varpi\partial_t\partial_\alpha h + \frac{1}{4\pi}\langle\varpi\rangle\partial_t\partial_\alpha^2 h\\
&\approx \frac{1}{4\pi}\partial_\alpha^2 h \frac{d}{dt}\langle\varpi\rangle - \frac{1}{2} H\varpi\partial_t\partial_\alpha h + \frac{1}{4\pi}\langle\varpi\rangle\partial_t\partial_\alpha^2 h.
\end{aligned}$$

If we neglect terms of order $O(h^2)$ in (15) and (16), we find that

$$h_t(\alpha,t) = \frac{1}{2} H\varpi\,, \tag{19a}$$

$$\begin{aligned}
\varpi_t(\alpha,t) &= 2Ag\partial_\alpha h + \frac{2\sigma}{\rho^+ + \rho^-}\partial_\alpha^3 h\\
&\quad + \frac{A}{2}\varpi\partial_\alpha\varpi + \partial_\alpha\left(\frac{\varpi}{2}\partial_\alpha h\, H\varpi \right) - \partial_\alpha\left(\frac{\varpi}{4\pi}\partial_\alpha^2 h \right)\langle\varpi\rangle\\
&\quad + \frac{A}{4\pi}\partial_\alpha\Lambda\varpi\langle\varpi\rangle - \frac{A}{2} H\varpi\Lambda\varpi + \frac{A}{2\pi}\partial_\alpha^2 h(\alpha)\frac{d}{dt}\langle\varpi\rangle\,.
\end{aligned} \tag{19b}$$

Integrating in space, we obtain that the vorticity average $\langle\varpi\rangle$ verifies

$$\frac{d}{dt}\langle\varpi\rangle = 0;$$

thus,

$$\langle\varpi\rangle(t) = \langle\varpi\rangle(0) = \langle\varpi_0\rangle.$$

Finally, we can use the Tricomi relation for the Hilbert transform,

$$2H(fHf) = (Hf)^2 - f^2\,, \tag{20}$$

to obtain

$$\frac{1}{2}\partial_\alpha((H\varpi)^2 - \varpi^2) = H\varpi\Lambda\varpi - \varpi\partial_\alpha\varpi = \partial_\alpha H(\varpi H\varpi).$$

Then, the system (19a), (19b) is equivalent to

$$h_t(\alpha,t) = \frac{1}{2}H\varpi\,, \tag{21a}$$

$$\begin{aligned}\varpi_t(\alpha,t) = {} & 2Ag\partial_\alpha h + \frac{2\sigma}{\rho^+ + \rho^-}\partial_\alpha^3 h + \partial_\alpha\left(\frac{\varpi}{2}\partial_\alpha h\, H\varpi\right) \\ & - \partial_\alpha\left(\frac{\varpi}{4\pi}\partial_\alpha^2 h\right)\langle\varpi_0\rangle + \frac{A}{4\pi}\partial_\alpha\Lambda\varpi\langle\varpi_0\rangle - \frac{A}{2}\Lambda(\varpi H\varpi)\,.\end{aligned} \tag{21b}$$

The coupled first-order system (21) can be written as one second-order equation for the evolution of the height function:

$$\begin{aligned}h_{tt}(\alpha,t) = {} & Ag\Lambda h - \frac{\sigma}{\rho^+ + \rho^-}\Lambda^3 h - \Lambda\left(Hh_t\partial_\alpha h\, h_t\right) \\ & - A\partial_\alpha(Hh_t h_t) + \Lambda\left(\frac{Hh_t}{4\pi}\partial_\alpha^2 h\right)\langle\varpi_0\rangle + \frac{A}{4\pi}\partial_\alpha\Lambda h_t\langle\varpi_0\rangle\,.\end{aligned} \tag{22}$$

The model equation (22) contains both quadratic and cubic nonlinearities, but we can simplify further.

Keeping only the quadratic nonlinearities, we find that the graph of the interface $(x, h(x,t))$ evolves according to

$$\begin{aligned}h_{tt}(\alpha,t) = {} & Ag\Lambda h - \frac{\sigma}{\rho^+ + \rho^-}\Lambda^3 h \\ & - A\partial_\alpha(Hh_t h_t) + \Lambda\left(\frac{Hh_t}{4\pi}\partial_\alpha^2 h\right)\langle\varpi_0\rangle + \frac{A}{4\pi}\partial_\alpha\Lambda h_t\langle\varpi_0\rangle\,.\end{aligned} \tag{23}$$

By assuming that our initial vorticity has zero average, we arrive at the nonlinear equation

$$h_{tt}(\alpha,t) = Ag\Lambda h - \frac{\sigma}{\rho^+ + \rho^-}\Lambda^3 h - A\partial_\alpha(Hh_t h_t)\,. \tag{24}$$

Equation (24) is supplemented with initial conditions. In particular, we specify the initial interface position and velocity, respectively, by

$$h(\cdot,0) = h_0 \quad \text{and } h_t(\cdot,t) = h_1\,.$$

As we explain in the next section, this model equation has a natural stability condition, requiring the product of the Atwood number A and the initial velocity field h_1 to be positive.

The second-order–in-time nonlinear wave equation (24) is a new model for the motion of an interface under the influence of RT instability. We shall refer to either the system (21) or the wave equation (24) as the h-model.

Remark 6.1. The quadratic nonlinearity $u \mapsto \partial_\alpha(u\,Hu)$ has been previously studied by many authors (see, for instance, [1, 2, 3, 4, 5]). In those papers, the model problem was parabolic and thus yielded a maximum principle, from which many of the analytical results followed. Our study of (24) involves a hyperbolic-type problem with no maximum principle. Of particular significance of the structure of (24) is the recovery of an RT-like stability condition for the model; this will be discussed in great detail next.

7. Well-posedness of the *h*-model equation (24). We now prove that our h-model equation (24) is well-posed in Sobolev spaces, when a certain stability condition is satisfied by the data.

In this section we consider the periodic Hilbert transform H, defined as

$$Hf(\alpha) = \frac{1}{2\pi} P.V. \int_{\mathbb{T}} \frac{f(\beta)}{\tan\left(\frac{\alpha-\beta}{2}\right)} d\beta\,, \tag{25}$$

and the periodic Zygmund operator

$$\Lambda f(\alpha) = H\partial_\alpha f(\alpha) = \frac{1}{4\pi} P.V. \int_{\mathbb{T}} \frac{f(\alpha)-f(\beta)}{\sin^2\left(\frac{\alpha-\beta}{2}\right)} d\beta\,. \tag{26}$$

Recall also that $\Lambda = (-\Delta)^{\frac{1}{2}}$.

The space $L^2(\mathbb{T})$ consists of the Lebesgue measurable functions on the circle $\mathbb{T}$ which are square integrable with norm $\|h\|_0^2 = \int_{\mathbb{T}} |h|^2 dx$. For $s \geq 0$, we define the homogeneous Sobolev space

$$\dot{H}^s(\mathbb{T}) = \left\{ h \in L^2(\mathbb{T}) \ : \ \sum_{k\in\mathbb{Z}} |k|^{2s} |\hat{h}(k)|^2 < \infty \right\},$$

with norm defined as

$$\|h\|_s^2 = \int_{\mathbb{T}} |\Lambda^s h|^2 dx\,. \tag{27}$$

For $s \geq 0$, functions $\dot{H}^s(\mathbb{T})$ are identified with 2π-periodic functions $[-\pi, \pi]$ with finite norm $\|\cdot\|_s$.

From (24),

$$\langle h_t(t) \rangle = \langle h_1 \rangle.$$

Thus,

$$\frac{d}{dt}\langle h(t)\rangle = \int_{\mathbb{T}} h_t(t) dx = \langle h_1 \rangle,$$

so that

$$\langle h(t)\rangle = \langle h_0\rangle + \langle h_1\rangle t.$$

These identities show that given $h_0 \in L^2(\mathbb{T})$, it follows that $h(\cdot, t) \in L^2(\mathbb{T})$, and so together with the Poincaré inequality, control of the seminorm (27) provides full $H^s(\mathbb{T})$ bounds for h. (Recall that we are using the notation $\langle f\rangle(t)$ to denote $\int f(\beta, t) d\beta$ for any integrable function $f(\beta, t)$.)

THEOREM 7.1 (local well-posedness for the h-model (24)). *Let $\sigma \geq 0$, $\rho^+, \rho^- > 0$, $g \neq 0$ be fixed constants and let (h_0, h_1) denote the initial position and velocity pair for (24). Suppose that $(h_0, h_1) \in H^{2.5+sgn(\sigma)}(\mathbb{T}) \times H^2(\mathbb{T})$ and let*

$$\lambda := \min_{\alpha \in \mathbb{T}} A\, h_1(\alpha). \tag{28}$$

If

$$\lambda > 0\,, \tag{29}$$

then there exists a time $0 < T^*(h_0, h_1) \leq \infty$ and a unique classical solution of (24) satisfying

$$h \in C^0([0, T^*]; H^{2.5+sgn(\sigma)}),\ h_t \in C^0([0, T^*]; H^2) \cap L^2(0, T^*; H^{2.5}).$$

Proof. Step 1. *Approximate problem for h^ϵ, $\epsilon > 0$.* For $\epsilon > 0$, we introduce a sequence of approximations to (24). We let P_ϵ denote the projection operator in $L^2(\mathbb{T})$, given by

$$P_\epsilon f(\alpha) = \sum_{|k| \leq 1/\epsilon} \hat{f}(k) e^{ik\alpha}\,,$$

where $\hat{f}(k)$ denotes the kth Fourier mode of f. Then, we let h^ϵ be a solution to

$$h^\epsilon_{tt}(\alpha, t) = Ag P_\epsilon \Lambda P_\epsilon h^\epsilon - \frac{\sigma}{\rho^+ + \rho^-} P_\epsilon \Lambda^3 P_\epsilon h^\epsilon - A P_\epsilon \partial_\alpha (P_\epsilon h^\epsilon_t\, P_\epsilon H h^\epsilon_t) \tag{30}$$

with initial data given by $(P_\epsilon h_0, P_\epsilon h_1)$. The projection operator P_ϵ commutes with ∂_α and with H (and hence with Λ).

We let the parameter ϵ range in the interval $(0, \epsilon_0]$ for a constant $\epsilon_0 \ll 1$ to be chosen later. Then, ODE theory provides a unique short-time solution h^ϵ to (30) on a time interval $[0, T_\epsilon]$; the solution h_ϵ is smooth and can be taken in $C^2([0, T_\epsilon]; H^s(\mathbb{T}))$ for all $s \geq 0$.

According to (30), $h^\epsilon_{tt} = P_\epsilon h^\epsilon_{tt}$; since $(h^\epsilon(0), h^\epsilon_t(0)) = (P_\epsilon h_0, P_\epsilon h_1)$, the fundamental theorem of calculus shows that

$$h^\epsilon = P_\epsilon h^\epsilon \ \text{ and } \ h^\epsilon_t = P_\epsilon h^\epsilon_t\,.$$

As such, (30) can be written as

$$h^\epsilon_{tt}(\alpha, t) = Ag \Lambda P^2_\epsilon h^\epsilon - \frac{\sigma}{\rho^+ + \rho^-} \Lambda^3 P^2_\epsilon h^\epsilon - A P_\epsilon \partial_\alpha (h^\epsilon_t\, H h^\epsilon_t)\,. \tag{30$'$}$$

Step 2. *The higher-order energy norm.* We define the higher-order energy norm $E(t)$ by

$$E(t) = \sup_{0 \leq s \leq t} \left\{ \frac{\sigma}{\rho^+ + \rho^-} \|h^\epsilon(s)\|^2_{3.5} + \|h^\epsilon_t(s)\|^2_2 + \frac{\lambda}{2} \int_0^t \|h^\epsilon_t(s)\|^2_{2.5} ds \right\}. \tag{31}$$

Note that for each $\epsilon \in (0, \epsilon_0]$, $t \mapsto E(t)$ is continuous on $[0, T^\epsilon]$.

Step 3. *Lower bound for h^ϵ_t.* We shall assume that by choosing T_ϵ and ϵ_0 sufficiently small,

$$A\, h^\epsilon_t(\alpha, t) \geq \frac{\lambda}{2} \ \forall\ \alpha \in \mathbb{T}, t \in [0, T_\epsilon], \epsilon \in [0, \epsilon_0]\,. \tag{32}$$

Below, we shall verify that this assumption holds on a time interval $[0,T]$, where T is independent of ϵ.

Step 4. ϵ-independent energy estimates. We now establish a time of existence and bounds for h^ϵ which are independent of ϵ.

We multiply (24) by $\Lambda^4 h_t^\epsilon$, integrate over $\mathbb{T}$, and find that

$$\frac{1}{2}\left(\frac{d}{dt}\|h_t^\epsilon\|_2^2 + \frac{\sigma}{\rho^+ + \rho^-}\frac{d}{dt}\|h^\epsilon\|_{3.5}^2\right) \leq |g|\|h^\epsilon\|_{2.5}\|h_t^\epsilon\|_{2.5} + I, \tag{33}$$

where

$$I = -A\int_{\mathbb{T}} \partial_\alpha(h_t^\epsilon H h_t^\epsilon)\,\partial_\alpha^4 h_t^\epsilon\,d\alpha. \tag{34}$$

We first write the integral I as

$$\begin{aligned} I &= -A\int_{\mathbb{T}} \partial_\alpha^3(h_t^\epsilon\, H h_t^\epsilon)\partial_\alpha^2 h_t^\epsilon d\alpha \\ &= \underbrace{-A\int_{\mathbb{T}} \Lambda\partial_\alpha^2 h_t^\epsilon\, h_t^\epsilon\,\partial_\alpha^2 h_t^\epsilon d\alpha}_{I_1} \underbrace{- A\int_{\mathbb{T}} H h_t^\epsilon\,\partial_\alpha^3 h_t^\epsilon\,\partial_\alpha^2 h_t^\epsilon d\alpha}_{I_2} \\ &\quad \underbrace{- 3A\int_{\mathbb{T}} \left[\Lambda\partial_\alpha h_t^\epsilon \partial_\alpha h_t^\epsilon + \Lambda h_t^\epsilon \partial_\alpha^2\right]\,\partial_\alpha^2 h_t^\epsilon d\alpha}_{I_3}\,. \end{aligned}$$

The integral I_2 has an exact derivative, so upon integration by parts,

$$I_2 = \frac{A}{2}\int_{\mathbb{T}} \Lambda h_t^\epsilon\,\partial_\alpha^2 h_t^\epsilon\,\partial_\alpha^2 h_t^\epsilon\,d\alpha \leq \|h_t^\epsilon\|_2^2\|\Lambda h_t^\epsilon\|_{L^\infty} \leq C\|h_t^\epsilon\|_2^2\|h_t^\epsilon\|_{1.75}\,,$$

the last inequality following from the Sobolev embedding theorem. The integral I_3 clearly has the same bound.

Equipped with the assumption (32) and the estimate for I_2, the integral I_1 provides extra regularity for h_t^ϵ as follows:

$$\begin{aligned} I_1 &= -\int_{\mathbb{T}}\left(\frac{1}{4\pi}\int_{\mathbb{T}} \frac{\partial_\alpha^2 h_t^\epsilon(\alpha) - \partial_\alpha^2 h_t^\epsilon(\beta)}{\sin^2\left(\frac{\alpha-\beta}{2}\right)}d\beta\right) A h_t^\epsilon(\alpha)\partial_\alpha^2 h_t^\epsilon(\alpha)d\alpha \\ &= \int_{\mathbb{T}}\left(\frac{1}{4\pi}\int_{\mathbb{T}} \frac{\partial_\alpha^2 h_t^\epsilon(\alpha) - \partial_\alpha^2 h_t^\epsilon(\beta)}{\sin^2\left(\frac{\alpha-\beta}{2}\right)}d\beta\right) A h_t^\epsilon(\beta)\partial_\alpha^2 h_t^\epsilon(\beta)d\alpha \\ &= -\frac{A}{8\pi}\int_{\mathbb{T}}\int_{\mathbb{T}} \frac{\partial_\alpha^2 h_t^\epsilon(\alpha) - \partial_\alpha^2 h_t^\epsilon(\beta)}{\sin^2\left(\frac{\alpha-\beta}{2}\right)}\left(h_t^\epsilon(\alpha)\partial_\alpha^2 h_t^\epsilon(\alpha) - h_t^\epsilon(\beta)\partial_\alpha^2 h_t^\epsilon(\beta)\right)d\alpha d\beta \\ &\leq -\frac{A}{8\pi}\int_{\mathbb{T}}\int_{\mathbb{T}} \frac{\left(\partial_\alpha^2 h_t^\epsilon(\alpha) - \partial_\alpha^2 h_t^\epsilon(\beta)\right)\left(h_t^\epsilon(\alpha) - h_t^\epsilon(\beta)\right)}{\sin^2\left(\frac{\alpha-\beta}{2}\right)}\partial_\alpha^2 h_t^\epsilon(\alpha)d\alpha d\beta \\ &\quad -\frac{A}{8\pi}\int_{\mathbb{T}}\int_{\mathbb{T}} \frac{\left(\partial_\alpha^2 h_t^\epsilon(\alpha) - \partial_\alpha^2 h_t^\epsilon(\beta)\right)^2}{\sin^2\left(\frac{\alpha-\beta}{2}\right)}h_t^\epsilon(\beta)d\alpha d\beta \\ &\leq -\frac{A}{8\pi}\int_{\mathbb{T}}\int_{\mathbb{T}} \frac{\left(\partial_\alpha^2 h_t^\epsilon(\alpha) - \partial_\alpha^2 h_t^\epsilon(\beta)\right)^2}{\sin^2\left(\frac{\alpha-\beta}{2}\right)}h_t^\epsilon(\beta)d\alpha d\beta + \frac{A}{2}\int_{\mathbb{T}}\Lambda h_t^\epsilon\,\partial_\alpha^2 h_t^\epsilon\,\partial_\alpha^2 h_t^\epsilon\,d\alpha\,. \end{aligned}$$

The last equality follows from the fact that

$$\int_{\mathbb{T}}\int_{\mathbb{T}} \frac{\partial_\alpha^2 h_t^\epsilon(\beta)\partial_\alpha^2 h_t^\epsilon(\alpha)\,(h_t^\epsilon(\alpha)-h_t^\epsilon(\beta))}{\sin^2\left(\frac{\alpha-\beta}{2}\right)}d\alpha d\beta = 0\,.$$

With our assumed lower bound for h_t^ϵ in (32), we find that

$$-I_1 \geq \frac{\lambda}{2}\frac{1}{8\pi}\int_{\mathbb{T}}\int_{\mathbb{T}} \frac{\left(\partial_\alpha^2 h_t^\epsilon(\alpha)-\partial_\alpha^2 h_t^\epsilon(\beta)\right)^2}{\sin^2\left(\frac{\alpha-\beta}{2}\right)}d\alpha d\beta\,.$$

Using the computation

$$\begin{aligned}\int_{\mathbb{T}} f\Lambda f d\alpha &= \int_{\mathbb{T}}\left(\frac{1}{4\pi}\int_{\mathbb{T}}\frac{f(\alpha)-f(\beta)}{\sin^2\left(\frac{\alpha-\beta}{2}\right)}d\beta\right)f(\alpha)d\alpha\\ &= -\int_{\mathbb{T}}\frac{1}{4\pi}\int_{\mathbb{T}}\frac{f(\alpha)-f(\beta)}{\sin^2\left(\frac{\alpha-\beta}{2}\right)}f(\beta)d\beta d\alpha\\ &= \frac{1}{8\pi}\int_{\mathbb{T}}\int_{\mathbb{T}}\frac{(f(\alpha)-f(\beta))^2}{\sin^2\left(\frac{\alpha-\beta}{2}\right)}d\beta d\alpha\,,\end{aligned}$$

it follows that $I_1 \leq -\frac{\lambda}{2}\|h_t^\epsilon\|_{2.5}^2$ and, hence,

$$I \leq -\frac{\lambda}{2}\|h_t^\epsilon\|_{2.5}^2 + C\|h_t^\epsilon\|_2^2\|h_t^\epsilon\|_{1.75}\,.$$

Thus,

(35)
$$\frac{1}{2}\left(\frac{d}{dt}\|h_t^\epsilon\|_2^2 + \frac{\sigma}{\rho^+ + \rho^-}\frac{d}{dt}\|h^\epsilon\|_{3.5}^2\right) \leq |g|\|h^\epsilon\|_{2.5}\|h_t^\epsilon\|_{2.5} - \frac{\lambda}{2}\|h_t^\epsilon\|_{2.5}^2 + C\|h_t^\epsilon\|_2^2\|h_t^\epsilon\|_{1.75}.$$

The fundamental theorem of calculus shows that

$$\|h^\epsilon\|_{2.5}^2 \leq \|h_0\|_{2.5}^2 + t\int_0^t \|h_t^\epsilon(s)\|_{2.5}^2 ds$$

and, hence,

$$\begin{aligned}\frac{d}{dt}\|h_t^\epsilon\|_2^2 + \frac{\sigma}{\rho^+ + \rho^-}\frac{d}{dt}\|h^\epsilon\|_{3.5}^2 + \frac{\lambda}{2}\|h_t^\epsilon\|_{2.5}^2 &\leq C\|h^\epsilon\|_{2.5}^2 + C\|h_t^\epsilon\|_2^4\\ &\leq C\|h_0\|_{2.5}^2 + Ct\int_0^t \|h_t^\epsilon\|_{2.5}^2 ds + C\|h_t^\epsilon\|_2^4\,.\end{aligned}$$

It follows that

$$\frac{d}{dt}E(t) \leq C\|h_t^\epsilon\|_2^2 E(t) + C\|h_0\|_{2.5} \leq CE(t)^2 + C\|h_0\|_{2.5}\,. \tag{36}$$

By Gronwall's inequality,

$$E(t) \leq C\left[\|h_0\|_{2.5}^2 + \|h_1\|_2^2\right]\,. \tag{37}$$

Step 5. *Verifying the lower-bound on h_t^ϵ.* As the bound (37) for $E(t)$ is independent of ϵ and σ, there exists a time interval $[0,T]$, with T independent of ϵ and σ, such that

$$E(t) \leq C\left[\|h_0\|_{2.5}^2 + \|h_1\|_2^2\right] \quad \text{on } [0,T] \text{ with } T \text{ independent of } \epsilon, \sigma\,. \tag{38}$$

Using (30′), we see that h_{tt}^ϵ is bounded in $L^2(0,T;L^2(\mathbb{T}))$. Thus,

$$\|h_t(T) - P_\epsilon h_1\|_{L^2} \leq \int_0^T \|h_{tt}(s)\|_{L^2} ds \leq C\,T.$$

Since $\|h_t(T) - P_\epsilon h_1\|_2 \leq C$, we can interpolate between the last two inequalities and use the Sobolev embedding theorem to conclude that

$$\left\|h_t(T^2) - P_\epsilon h_1\right\|_{L^\infty} \leq C T^{1/8}\,.$$

By choosing T and ϵ_0 sufficiently small, and using (28), we verify (32).

Step 6. *Existence of solutions.* From (38), for all $1 < p < \infty$,

$$\begin{aligned} &h^\epsilon \rightharpoonup h \ \text{ in } W^{1,p}(0,T;H^2(\mathbb{T}))\,,\\ &h_t^\epsilon \rightharpoonup h \ \text{ in } L^2(0,T;H^{2.5}(\mathbb{T})) \cap H^1(0,T;L^2(\mathbb{T})) \cap L^p(0,T;H^2(\mathbb{T}))\,. \end{aligned}$$

By using Rellich's theorem, we can pass to the limit as $\epsilon \to 0$ in (30′). Since $\|f\|_{L^\infty} = \lim_{p\to\infty} \|f\|_{L^p}$, we find that the limit h is a solution of (24) on $[0,T]$ and

$$h \in L^\infty(0,T;H^{2.5}(\mathbb{T}))\,,\ h_t \in L^2(0,T;H^{2.5}(\mathbb{T})) \cap L^\infty(0,T;H^2(\mathbb{R}))\,.$$

It is easy to prove that $t \mapsto h(\cdot,t)$ and $t \mapsto h_t(\cdot,t)$ are continuous into $H^{2.5}(\mathbb{T})$ and $H^2(\mathbb{T})$, respectively, with respect to the weak topologies on $H^{2.5}(\mathbb{T})$ and $H^2(\mathbb{T})$; furthermore, we can again find a differential inequality that is almost identical to (36) (but this time for the solution h rather than the sequence h^ϵ). It follows that $t \mapsto \|h(t)\|_{2.5}$ and $t \mapsto \|h_t(t)\|_{2.5}$ are continuous, hence

$$h \in C^0(0,T;H^{2.5}(\mathbb{T}))\,,\ h_t \in L^2(0,T;H^{2.5}(\mathbb{T})) \cap C^0(0,T;H^2(\mathbb{R}))\,.$$

When $\sigma > 0$, by the same argument, we have the better regularity

$$h \in C^0(0,T;H^{3.5}(\mathbb{T}))\,.$$

Step 7. *Uniqueness of solutions.* Uniqueness of solutions follows from a standard L^2-type energy estimate, and we omit the details. ∎

Remark 7.2. If the stability condition $A\,h_1 > 0$ is not satisfied, the evolution equation (24) may not be well-posed in Sobolev spaces. For analytic initial data, however, the equation does not require a stability condition for a short-time existence theorem. We shall investigate this further in future work.

Having established existence and uniqueness of classical solutions to the RT model (24), we next establish a number of interesting energy laws satisfied by its solutions.

PROPOSITION 7.3 (energy laws for solutions to the h-model (24)). *Given constants $\sigma \geq 0, \rho^+, \rho^- > 0$, and $g \neq 0$, suppose that h is a solution to* (24) *with initial*

data (h_0, h_1). *Then, with* T^* *given by Theorem* 7.1 *and for all* $0 \le t \le T^*$, h *verifies the following energy laws:*

$$\|h_t\|_0^2 + \frac{\sigma}{\rho^+ + \rho^-}\|h\|_{1.5}^2 - Ag\|h\|_{0.5}^2 + \int_0^t D_1(s)ds$$

(39a)

$$= \|h_1\|_0^2 + \frac{\sigma}{\rho^+ + \rho^-}\|h_0\|_{1.5}^2 - Ag\|h_0\|_{0.5}^2,$$

$$\|h_t\|_{0.5}^2 + \frac{\sigma}{\rho^+ + \rho^-}\|h\|_2^2 - Ag\|h\|_1^2 + \int_0^t D_2(s)ds$$

(39b)

$$= \|h_1\|_{0.5}^2 + \frac{\sigma}{\rho^+ + \rho^-}\|h_0\|_2^2 - Ag\|h_0\|_1^2,$$

$$\|h_t - \langle h_1\rangle\|_{-0.5}^2 + \frac{\sigma}{\rho^+ + \rho^-}\|h\|_1^2 - Ag\|h\|_0^2 + \int_0^t D_3(s)ds + 2Ag\int_0^t 2\langle h_1\rangle\langle h(s)\rangle ds$$

(39c)

$$= \|h_1 - \langle h_1\rangle\|_{-0.5}^2 + \frac{\sigma}{\rho^+ + \rho^-}\|h_0\|_1^2 - Ag\|h_0\|_0^2,$$

where the terms D_1, D_2, *and* D_3 *are given by*

$$D_1 = 2\int_{\mathbb{T}} P.V. \int_{\mathbb{T}} \frac{A\left(h_t(\alpha) + h_t(\beta)\right)\left(h_t(\alpha) - h_t(\beta)\right)^2}{8\pi \sin^2\left(\frac{\alpha-\beta}{2}\right)} d\alpha d\beta\,,$$

$$D_2 = A\int_{\mathbb{T}} h_t\left(\left(\Lambda h_t\right)^2 + \left(\partial_\alpha h_t\right)^2\right) d\alpha\,,$$

$$D_3 = 2A\int_{\mathbb{T}} h_t \left|Hh_t\right|^2 d\alpha\,.$$

Proof. The proof reduces to a careful manipulation of the following integrals:

$$I_1 = -A\int_{\mathbb{T}} \partial_\alpha(h_t H h_t) h_t d\alpha\,,$$

$$I_2 = -A\int_{\mathbb{T}} \partial_\alpha(h_t H h_t)\Lambda h_t d\alpha\,,$$

$$I_3 = -A\int_{\mathbb{T}} \partial_\alpha(h_t H h_t)\Lambda^{-1}(h_t - \langle h_1\rangle) d\alpha\,,$$

where $I_j = -D_j/2$ for $j = 1, 2, 3$. First,

$$\begin{aligned} I_1 &= A\int_{\mathbb{T}} H h_t h_t \partial_\alpha h_t d\alpha \\ &= -\frac{A}{2}\int_{\mathbb{T}} \Lambda h_t h_t^2 d\alpha \\ &= -\frac{A}{8\pi}\int_{\mathbb{T}} \text{P.V.} \int_{\mathbb{T}} \frac{(h_t(\alpha) - h_t(\beta))^2 (h_t(\alpha) + h_t(\beta))}{\sin^2\left(\frac{\alpha-\beta}{2}\right)} d\beta d\alpha. \end{aligned}$$

Next,

$$I_2 = -A\int_{\mathbb{T}} \partial_\alpha h_t H h_t \partial_\alpha H h_t h d\alpha - A\int_{\mathbb{T}} h_t \left|\Lambda h_t\right|^2 d\alpha.$$

Using the skew adjointness of the Hilbert transform and Tricomi relation (20),

$$-A\int_{\mathbb{T}} Hh_t\partial_\alpha h_t H\partial_\alpha h_t d\alpha = A\int_{\mathbb{T}} h_t H\left(\partial_\alpha h_t H\partial_\alpha h_t\right) d\alpha$$
$$= \frac{A}{2}\int_{\mathbb{T}} h_t\left(\left(\Lambda h_t\right)^2 - \left(\partial_\alpha h_t\right)^2\right) d\alpha,$$

so that

$$I_2 = -\frac{A}{2}\int_{\mathbb{T}} h_t\left(\left(\Lambda h_t\right)^2 + \left(\partial_\alpha h_t\right)^2\right) d\alpha.$$

Finally,

$$I_3 = -A\int_{\mathbb{T}} \Lambda^{-1}\partial_\alpha(h_t H h_t)(h_t - \langle h_1\rangle)d\alpha$$
$$= A\int_{\mathbb{T}} H(h_t H h_t)(h_t - \langle h_1\rangle)d\alpha$$
$$= -A\int_{\mathbb{T}} h_t\left|Hh_t\right|^2 d\alpha\,,$$

where we have used the fact that $\Lambda^{-1}\partial_\alpha = -H$, so that $H\partial_\alpha = \Lambda$. ∎

COROLLARY 7.4. *If $\rho_+ < \rho^-$ so that the Atwood number $A < 0$, and if gravity acts downward so that $g > 0$, then whenever the initial velocity h_1 satisfies the stability condition $h_1 < 0$, the energy law* (39b) *shows that*

$$\|h_t(t)\|_{0.5}^2 + \frac{\sigma}{\rho^+ + \rho^-}\|h(t)\|_2^2 + |Ag|\|h(t)\|_1^2 \quad \textit{decays in time } \forall t \in [0, T^*]\,,$$

where T^* is given by Theorem 7.1.

Remark 7.5. The energy law (39a) provides decay for lower-order norms when $A\,h_1 > 0$, while the energy law (39c) may actually cause a growth in time which behaves like t^2. There may indeed be other higher-order energy laws to the model equation (24) that have yet to be established.

We now define the average value of a function $h(\alpha)$ on $[-\pi, \pi]$:

$$\bar{h} := \frac{\langle h\rangle}{2\pi} = \frac{1}{2\pi}\int_{\mathbb{T}} h(\alpha)d\alpha\,.$$

THEOREM 7.6 (global well-posedness and asymptotic behavior for the h-model (24)). *Let $\sigma \geq 0$, $\rho^+, \rho^- > 0$, $g \neq 0$ be fixed constants such that $Ag < 0$, and let (h_0, h_1) denote the initial position and velocity, respectively, for the h-model* (24). *Setting*

$$h_2 := h_{tt}(\cdot, 0) = Ag\Lambda h_0 + \sigma\Lambda^3 h_0 - A\partial_\alpha(Hh_1h_1)\,,$$

and with λ defined by (28), *suppose that $(h_0, h_1) \in H^{2.5+sgn(\sigma)}(\mathbb{T}) \times H^2(\mathbb{T})$ is given such that*

$$\lambda > 0 \tag{40}$$

and

$$\|h_2\|_{0.5}^2 + \|h_1\|_1^2 + \sigma\|h_1\|_2^2 < \left(\frac{\bar{h}_1}{5}\right)^2\,. \tag{41}$$

Then there exists a unique classical solution of (24) *satisfying*

$$h \in C^0([0,T]; H^{2.5+sgn(\sigma)}),\ h_t \in C^0([0,T]; H^2) \cap L^2(0,T; H^{2.5})\ \forall\, 0 \le T < \infty.$$

Furthermore, as $t \to \infty$*, the solution* $h(\cdot,t)$ *converges to the homogeneous solution* $h^\infty = \bar{h}_0 + \bar{h}_1 t$*; specifically,*

$$\limsup_{t\to\infty} \|h(t) - h^\infty\|_{1+sgn(\sigma)} + \|h_t(t) - \bar{h}_1\|_{1+sgn(\sigma)} = 0.$$

Proof. Without loss of generality, we consider $\rho^+ = 0$, $\rho^- = 1$, and $g = 1$ so that $A = -1$. Our analysis will rely on the fact that

$$\langle h_1 \rangle < 0\,,$$

since we have assumed the initial velocity satisfies $h_1 < 0$.

It is convenient to introduce a new variable $f(\alpha,t)$ given by

$$f = h - \bar{h}_0 - \bar{h}_1 t \ \text{ so that } \ f_t = h_t - \bar{h}_1.$$

It follows that f satisfies the evolution equation

$$f_{tt}(\alpha,t) + \Lambda f + \sigma\Lambda^3 f - \bar{h}_1 \Lambda f_t = \partial_\alpha (H f_t f_t)\,, \tag{42}$$

with initial data

$$f_0 = h_0 - \bar{h}_0,\ f_1 = h_1 - \bar{h}_1.$$

The local existence for h and h_t (and, consequently, for f and f_t) follows from Theorem 7.1. Thus, in order to prove that solutions exist for all time, it remains only to establish estimates which are uniform in time, and the desired asymptotic behavior will be established by showing that both f and f_t converge to zero.

With λ defined by (28), the stability condition (40) for h_t reduces to

$$\sup_{0\le t} \|f_t(t)\|_{L^\infty} < -\bar{h}_1. \tag{43}$$

Furthermore, we have that

$$\int_{\mathbb{T}} f(\alpha,t) d\alpha = 0 \ \text{ and } \ \int_{\mathbb{T}} f_t(\alpha,t) d\alpha = 0\ \forall\, t \ge 0.$$

We tested (42) against Λf_t and obtained that

$$\begin{aligned}\frac{1}{2}\frac{d}{dt}\left(\|f_t\|_{0.5}^2 + \|f\|_1^2 + \sigma\|f\|_2^2\right) - \bar{h}_1\|f_t\|_1^2 &= \int_{\mathbb{T}} \partial_\alpha(H f_t f_t)\Lambda f_t d\alpha \\ &\le \|f_t\|_1^2(\|f_t\|_{L^\infty} + \|H f_t\|_{L^\infty}).\end{aligned}$$

We shall make use of the refined Carlson inequality [9]:

$$\|w\|_{L^\infty}^2 \le \|w\|_0\|w\|_1 - \frac{1}{\pi}\|w\|_0^2 \ \ \forall w \in \dot{H}^1(\mathbb{T}) \ \text{ with } \ \langle w \rangle = 0\,. \tag{44}$$

Using (44) together with the Poincaré inequality shows that

$$\|w\|_{L^\infty} < \|w\|_1.$$

As a consequence, we obtain that

$$\frac{1}{2}\frac{d}{dt}\left(\|f_t\|_{0.5}^2+\|f\|_1^2+\sigma\|f\|_2^2\right)-\bar{h}_1\|f_t\|_1^2<2\|f_t\|_1^3. \tag{45}$$

Taking a time derivative of (42), we find that f_t satisfies

$$f_{ttt}(\alpha,t)+\Lambda f_t+\sigma\Lambda^3 f_t-\bar{h}_1\Lambda f_{tt}=\partial_\alpha(Hf_{tt}f_t+Hf_tf_{tt}) \tag{46}$$

with initial data given by

$$f_1(\alpha)=f_t(\alpha,0),\ f_2=f_{tt}(\alpha,0)=-\Lambda f_0-\sigma\Lambda^3 f_0+\bar{h}_1\Lambda f_1+\partial_\alpha(Hf_1f_1)\,.$$

Testing (46) against Λf_{tt}, and using (44), we obtain that

$$\begin{aligned}\frac{1}{2}\frac{d}{dt}\left(\|f_{tt}\|_{0.5}^2+\|f_t\|_1^2+\sigma\|f_t\|_2^2\right)-\bar{h}_1\|f_{tt}\|_1^2&\leq\|f_{tt}\|_1^2(\|f_t\|_{L^\infty}+\|Hf_t\|_{L^\infty})\\&\quad+\|f_{tt}\|_1\|f_t\|_1(\|f_{tt}\|_{L^\infty}+\|Hf_{tt}\|_{L^\infty})\\&<4\|f_{tt}\|_1^2\|f_t\|_1.\end{aligned} \tag{47}$$

Next, we define the following energy and dissipation functions, respectively, as

$$E(t)=\|f_{tt}\|_{0.5}^2+\|f_t\|_1^2+\sigma\|f_t\|_2^2,\quad D(t)=-2\bar{h}_1\|f_{tt}\|_1^2\,.$$

Then (47) can be written as

$$\frac{d}{dt}E(t)+D(t)\leq\frac{4\sqrt{E(t)}}{-\bar{h}_1}D(t),$$

and we find decay of the energy

$$E(t)+\left(1-\frac{4\sqrt{E(0)}}{-\bar{h}_1}\right)\int_0^t D(s)ds\leq E(0),$$

provided that the initial data satisfy

$$E(0)<\left(\frac{-\bar{h}_1}{4}\right)^2.$$

Consequently, due to (41), the initial data f_0 and f_1 satisfy

$$E(0)=\|f_2\|_{0.5}^2+\|f_1\|_1^2+\sigma\|f_1\|_2^2<\left(\frac{-\bar{h}_1}{5}\right)^2, \tag{48}$$

and we have that (45) and (47) reduce to

$$\begin{aligned}\frac{d}{dt}\left(\|f_t\|_{0.5}^2+\|f\|_1^2+\sigma\|f\|_2^2\right)-\bar{h}_1\|f_t\|_1^2<0,\\ \frac{d}{dt}\left(\|f_{tt}\|_{0.5}^2+\|f_t\|_1^2+\sigma\|f_t\|_2^2\right)-\frac{2\bar{h}_1}{5}\|f_{tt}\|_1^2<0.\end{aligned}$$

Thus, we find the estimates

$$\|f_t(t)\|_{0.5}^2+\|f(t)\|_1^2+\sigma\|f(t)\|_2^2-\bar{h}_1\int_0^t\|f_t(s)\|_1^2ds\leq\|f_1\|_{0.5}^2+\|f_0\|_1^2+\sigma\|f_0\|_2^2,$$

$$\|f_{tt}(t)\|_{0.5}^2+\|f_t(t)\|_1^2+\sigma\|f_t(t)\|_2^2-\frac{2\bar{h}_1}{5}\int_0^t\|f_{tt}(s)\|_1^2ds\leq\|f_2\|_{0.5}^2+\|f_1\|_1^2+\sigma\|f_1\|_2^2,$$

and the asymptotic behavior

$$\limsup_{t\to\infty} \|f(t)\|_{1+\mathrm{sgn}(\sigma)} + \|f_t(t)\|_{1+\mathrm{sgn}(\sigma)} + \|f_{tt}(t)\|_{0.5} = 0. \tag{49}$$

Finally, using (44) and (48), we conclude that

$$\|f_t(t)\|_{L^\infty}^2 < \|f_t(t)\|_1^2 < \left(\frac{-\bar{h}_1}{5}\right)^2, \tag{50}$$

and the stability condition (43) is satisfied even in a stricter sense. Finally, we test (42) against $\Lambda^4 f_t$. We find that

$$\frac{1}{2}\frac{d}{dt}\left(\|f_t\|_2^2 + \|f\|_{2.5}^2 + \sigma\|f\|_{3.5}^2\right) - \bar{h}_1\|f_t\|_{2.5}^2 = \int_{\mathbb{T}} \partial_\alpha(f_t H f_t)\partial_\alpha^4 f_t d\alpha.$$

Using integration by parts, Sobolev embedding, and interpolation, we have that

$$\begin{aligned}
I &= \int_{\mathbb{T}} \partial_\alpha(f_t H f_t)\partial_\alpha^4 f_t d\alpha \\
&= -\int_{\mathbb{T}} \partial_\alpha^2(f_t H f_t)\partial_\alpha^3 f_t d\alpha \\
&= \frac{1}{2}\int_{\mathbb{T}} \partial_\alpha^2 f_t \Lambda f_t \partial_\alpha^2 f_t d\alpha - 2\int_{\mathbb{T}} \partial_\alpha f_t \Lambda f_t \partial_\alpha^3 f_t d\alpha + \int_{\mathbb{T}} \Lambda^{0.5}(f_t\partial_\alpha\Lambda f_t)\partial_\alpha\Lambda^{1.5} f_t d\alpha \\
&\le C\|f_t\|_{2.25}^2\|f_t\|_1 + \int_{\mathbb{T}} [\Lambda^{0.5}, f_t]\partial_\alpha\Lambda f_t \partial_\alpha\Lambda^{1.5} f_t + \int_{\mathbb{T}} f_t\partial_\alpha\Lambda^{1.5} f_t \partial_\alpha\Lambda^{1.5} f_t d\alpha \\
&\le C\|f_t\|_{2.5}\left(\|f_t\|_2\|f_t\|_1 + \|\partial_\alpha f_t\|_{L^4}\|\partial_\alpha\Lambda^{0.5} f_t\|_{L^4} + \|\Lambda^{0.5} f_t\|_{L^4}\|\partial_\alpha^2 f_t\|_{L^4}\right) \\
&\quad + \|f_t\|_{L^\infty}\|f_t\|_{2.5}^2 \\
&\le C\|f_t\|_{2.5}\left(\|f_t\|_2\|f_t\|_1 + \|f_t\|_{0.75}\|f_t\|_{2.25}\right) + \|f_t\|_{L^\infty}\|f_t\|_{2.5}^2,
\end{aligned}$$

where we have used the classical commutator estimate [10]

$$\|[\Lambda^{0.5}, u]v\|_{L^2} \le C(\|\partial_\alpha u\|_{L^4}\|\Lambda^{-0.5} v\|_{L^4} + \|\Lambda^{0.5} u\|_{L^4}\|v\|_{L^4}).$$

Using Young's inequality and (50), we find that

$$\frac{d}{dt}\left(\|f_t\|_2^2 + \|f\|_{2.5}^2 + \sigma\|f\|_{3.5}^2\right) + \delta\|f_t\|_{2.5}^2 \le C_1(h_0, h_1)\|f_t\|_2^2 \tag{51}$$

for a certain explicit $0 < \delta(h_0, h_1)$. Using Gronwall's inequality, we conclude that

$$\|f_t(t)\|_2^2 + \|f(t)\|_{2.5}^2 + \sigma\|f(t)\|_{3.5}^2 \le C_2(h_0, h_1)e^{C_1(h_0,h_1)t}. \tag{52}$$

Finally, from the regularity of f and f_t, we conclude the regularity of h and h_t. ∎

Remark 7.7. Let us emphasize that the condition (41) does *not* require *small* initial data; rather, we require that the homogeneous norms of the initial acceleration and velocity be comparable to the size of the average velocity. For example, in the case that surface tension $\sigma = 0$, we can consider

$$h_0 = A + Be^{\alpha i} \quad \text{and} \quad h_1 = -1000 + \frac{e^{\alpha i}}{6}$$

for constants A and B. A simple computation using the explicit form of h_0 and h_1 shows that the condition (41) is satisfied when $B \le 110$ and any A.

Remark 7.8. Finally, we note that the asymptotic condition (49) remains true for higher-order Sobolev norms if the condition (50) is replaced with further constraints on the initial data involving higher-order time derivatives of h evaluated at $t = 0$. In particular, we do not claim that (52) is sharp.

8. General interface parameterization with interface turnover. Our h-model equation (24) for the evolution of the height function $h(\alpha, t)$ uses a special parameterization in which the interface $\Gamma(t)$ is constrained to be the graph $(\alpha, h(\alpha, t))$. While this model works well in predicting the mixing layer, in the unstable regime and when the RT instability is initiated, the height function $h(\alpha, t)$ can only grow in amplitude. Our goal is to generalize the h-model equation (24) by using a general parameterization $z(\alpha, t)$ that permits the interface to turn over. As we will show, the ability for the wave to turn over, rather than only grow in amplitude, provides an even more accurate prediction of the RT mixing layer, at the expense of a slightly more complicated system of evolution equations.

We now return to the general evolution equations (10) and (11) and set $c(\alpha, t) = 0$; hence, the average velocity at the interface is

$$u(z(\alpha,t),t) = \frac{1}{2\pi}\int \varpi(\beta)\frac{(z(\alpha,t)-z(\beta,t))^{\perp}}{|z(\alpha,t)-z(\beta,t)|^2}d\beta$$

and the interface parameterization $z(\alpha, t) = (z_1(\alpha, t), z_2(\alpha, t))$ evolves according to

$$z_t(\alpha,t) = \frac{1}{2\pi}\int \varpi(\beta)\frac{(z(\alpha,t)-z(\beta,t))^{\perp}}{|z(\alpha,t)-z(\beta,t)|^2}d\beta\,, \tag{53}$$

while the vorticity amplitude satisfies

$$\begin{aligned}\varpi_t = -\partial_\alpha\Bigg[A\left|\frac{1}{2\pi}\int \varpi(\beta)\frac{(z(\alpha,t)-z(\beta,t))^{\perp}}{|z(\alpha,t)-z(\beta,t)|^2}d\beta\right|^2 \\ - \frac{A}{4}\frac{\varpi(\alpha,t)^2}{|\partial_\alpha z(\alpha,t)|^2} - \frac{2[\![p]\!]}{\rho^+ + \rho^-} - 2Agz_2\Bigg] \\ + \frac{A}{\pi}\partial_t\left[\int \varpi(\beta)\frac{(z(\alpha,t)-z(\beta,t))^{\perp}}{|z(\alpha,t)-z(\beta,t)|^2}\cdot\partial_\alpha z(\alpha,t)d\beta\right].\end{aligned} \tag{54}$$

For $\delta > 0$ taken sufficiently small, we define an approximate velocity field $\tilde{u}$ by

$$\tilde{u}(z(\alpha),t) = \frac{1}{\pi}\text{P.V.}\int_{\alpha-\delta}^{\alpha+\delta}\frac{\varpi(\beta)}{\alpha-\beta}\frac{\frac{(z(\alpha)-z(\beta))^{\perp}}{\alpha-\beta}}{\frac{|z(\alpha)-z(\beta)|^2}{(\alpha-\beta)^2}}d\beta. \tag{55}$$

Thus, it is evident that in our definition of the approximate velocity field $\tilde{u}$ (which depends on δ), we have restricted the *nonlocality* to a radius $\delta > 0$.

Using the difference quotient approximation for the derivative, $(\alpha-\beta)^{-1}(z(\alpha)-z(\beta)) \approx \partial_\alpha z(\alpha)$, the integrand in (55) can be approximated as

$$\frac{\varpi(\beta)}{\alpha-\beta}\frac{\frac{(z(\alpha)-z(\beta))^{\perp}}{\alpha-\beta}}{\frac{|z(\alpha)-z(\beta)|^2}{(\alpha-\beta)^2}} \approx \frac{\varpi(\beta)}{\alpha-\beta}\frac{\partial_\alpha^{\perp} z(\alpha)}{|\partial_\alpha z(\alpha)|^2}$$

if $\delta > 0$ is small enough. With the integrand approximated in this way and using the definition of the Hilbert transform, we define the *model velocity*

$$u_{mod}(z(\alpha,t),t) = \frac{1}{2}H\varpi(\alpha)\frac{(\partial_\alpha z(\alpha))^{\perp}}{|\partial_\alpha z(\alpha)|^2}. \tag{56}$$

To estimate the error in the approximation of the actual velocity u by the model velocity u_{mod}, we define

$$m = \min |\partial_\alpha z|,\ M = \max |\partial_\alpha z|.$$

Note that

$$z(\alpha) - z(\alpha-\beta) = \int_0^1 \partial_s z(\alpha + (s-1)\beta) ds = \beta \int_0^1 \partial_\alpha z(\alpha + (s-1)\beta) ds\,,$$

so that

$$m \le \frac{|z(\alpha) - z(\alpha-\beta)|}{|\beta|} \le M.$$

For any $r > 0$, we compute the difference of the two velocities as follows:

$$\begin{aligned} &u(z(\alpha),t) - u_{mod}(z(\alpha),t) \\ &\quad = \frac{1}{\pi}\text{P.V.} \int_{B_r(0)} \frac{\varpi(\alpha-\beta)}{\beta} \left[\frac{\frac{(z(\alpha)-z(\alpha-\beta))^\perp}{\beta}}{\frac{|z(\alpha)-z(\alpha-\beta)|^2}{\beta^2}} - \frac{\partial_\alpha^\perp z(\alpha)}{|\partial_\alpha z(\alpha)|^2} \right] d\beta \\ &\qquad + \frac{1}{\pi}\text{P.V.} \int_{B_r^c(0)} \frac{\varpi(\alpha-\beta)}{\beta} \left[\frac{\frac{(z(\alpha)-z(\alpha-\beta))^\perp}{\beta}}{\frac{|z(\alpha)-z(\alpha-\beta)|^2}{\beta^2}} - \frac{\partial_\alpha^\perp z(\alpha)}{|\partial_\alpha z(\alpha)|^2} \right] d\beta. \end{aligned}$$

By estimating each integral separately, and computing the minimum value the integral bounds as a function of $r > 0$, we find that

$$|u(z(\alpha),t) - u_{mod}(z(\alpha),t)| \le 2\frac{\|\varpi\|_{L^2}}{\pi} \left(\frac{1}{m^2} + 2 \right)^{0.5} \frac{\|\partial_\alpha^2 z\|_{L^\infty}^{0.5}}{m^{0.5}}\,. \tag{57}$$

The inequality (57) shows that when the curvature of the interface is smaller than the slope of the interface, a good approximation for the velocity is given by

$$\frac{1}{2\pi} \int \varpi(\beta) \frac{(z(\alpha,t) - z(\beta,t))^\perp}{|z(\alpha,t) - z(\beta,t)|^2} d\beta \approx \frac{1}{2} H\varpi(\alpha) \frac{(\partial_\alpha z(\alpha))^\perp}{|\partial_\alpha z(\alpha)|^2}. \tag{58}$$

Substituting (58) into (53) and (54), and using the Tricomi relation (20), we obtain the (more general) RT model evolution equations which allow for wave turnover:

$$z_t(\alpha,t) = \frac{1}{2} H\varpi(\alpha,t) \frac{(\partial_\alpha z(\alpha,t))^\perp}{|\partial_\alpha z(\alpha,t)|^2}\,, \tag{59a}$$

$$\varpi_t(\alpha,t) = -\partial_\alpha \left[\frac{A}{2} \frac{1}{|\partial_\alpha z(\alpha,t)|^2} H\left(\varpi(\alpha,t) H\varpi(\alpha,t)\right) - \frac{2[\![p]\!]}{\rho^+ + \rho^-} - 2Agz_2 \right]. \tag{59b}$$

Substituting the time derivative of (59a) into (59b) yields

$$\begin{aligned} z_{tt} = &-\Lambda \left[\frac{A}{4} \frac{1}{|\partial_\alpha z|^2} H\left(\varpi H\varpi\right) - \frac{[\![p]\!]}{\rho^+ + \rho^-} - Agz_2 \right] \frac{(\partial_\alpha z)^\perp}{|\partial_\alpha z|^2} \\ &+ \frac{1}{2} H\varpi \left(\frac{(\partial_\alpha z_t)^\perp}{|\partial_\alpha z|^2} - \frac{(\partial_\alpha z)^\perp 2(\partial_\alpha z \cdot \partial_\alpha z_t)}{|\partial_\alpha z|^4} \right). \end{aligned}$$

Notice that (59a) implies that

$$H\varpi = 2z_t \cdot (\partial_\alpha z)^\perp \text{ and } \varpi = -2H(z_t \cdot (\partial_\alpha z)^\perp). \tag{60}$$

Thus, we obtain the equivalent second-order nonlinear wave system for $z(\alpha,t)$ given by

$$z_{tt} = \Lambda\left[\frac{A}{|\partial_\alpha z|^2} H\left(z_t\cdot(\partial_\alpha z)^\perp H(z_t\cdot(\partial_\alpha z)^\perp)\right) + \frac{[\![p]\!]}{\rho^+ + \rho^-} + Agz_2\right]\frac{(\partial_\alpha z)^\perp}{|\partial_\alpha z|^2}$$
$$+ z_t\cdot(\partial_\alpha z)^\perp\left(\frac{(\partial_\alpha z_t)^\perp}{|\partial_\alpha z|^2} - \frac{(\partial_\alpha z)^\perp 2(\partial_\alpha z\cdot\partial_\alpha z_t)}{|\partial_\alpha z|^4}\right). \tag{61}$$

We shall refer to the system (59) or the wave equation (61) as the z-model. The z-model (61) is analogous to the slightly simpler h-model (24).

Remark 8.1. Note well that due to our choice of setting $c(\alpha,t)=0$, the evolving interface solving (59) (or equivalently (61)) does *not* remain a graph, even if the initial data $z(\alpha,0)=(\alpha,h_0(\alpha)), z_t(\alpha,0)=(0,h_1(\alpha))$ are given as graphs. In particular, it is convenient (especially for the purposes of comparing against the h-model (24)) to prescribe the initial interface position as a graph, and allow the interface to evolve into a nongraph state. As we will show, the z-model (59) captures the turnover of the RT interface.

9. Numerical study.

9.1. The algorithm. In order to stabilize numerical oscillations without affecting the amplitude or speed of wave propagation, we shall employ an arbitrary-order artificial viscosity operator for both the h-model (21) (or (24)) and the z-model (59) (or (61)).

9.1.1. Numerical approximation of the *h*-model. We first consider the h-model, written as a system in (21). We numerically discretize the following approximation:

$$h_t^\epsilon = \frac{1}{2}H\varpi^\epsilon, \tag{62a}$$
$$\varpi_t^\epsilon = 2Ag\partial_\alpha h^\epsilon + \frac{2\sigma}{\rho^+ + \rho^-}\partial_\alpha^3 h^\epsilon - \partial_\alpha\left(\frac{\varpi^\epsilon}{4\pi}\partial_\alpha^2 h^\epsilon\right)\langle\varpi_0\rangle$$
$$+ \frac{A}{4\pi}\partial_\alpha\Lambda\varpi^\epsilon\langle\varpi_0\rangle - \frac{A}{2}\Lambda(\varpi^\epsilon H\varpi^\epsilon) - \epsilon\Lambda^s\varpi^\epsilon, \tag{62b}$$

where $\epsilon>0$ is the artificial viscosity, and $s\geq 2$ determines the order of the artificial viscosity employed.

Equivalently, we have the approximation for the wave equation given by

$$\partial_t^2 h^\epsilon + \epsilon\Lambda^s h_t^\epsilon = Ag\Lambda h^\epsilon - \frac{\sigma}{\rho^+ + \rho^-}\Lambda^3 h^\epsilon - A\partial_\alpha(Hh_t^\epsilon h_t^\epsilon)$$
$$+ \Lambda\left(\frac{Hh_t^\epsilon}{4\pi}\partial_\alpha^2 h^\epsilon\right)\langle\varpi_0\rangle + \frac{A}{4\pi}\partial_\alpha\Lambda h_t^\epsilon\langle\varpi_0\rangle. \tag{63}$$

The term $\epsilon\Lambda^s h_t^\epsilon$ represents the artificial viscosity operator. The parameter s determines the order of the operator; for example, for $s=2$, we recover the classical Laplace operator, while for $s>2$, we can study a variety of hyperviscosity operators. We believe that this equation will be an ideal candidate for the C-method artificial viscosity which is localized in both space and time (see [14]), and shall implement this in future work.

We use a Fourier collocation method to solve (62). We note that for the numerical simulations that we consider herein, we choose initial data for which $\langle \varpi_0 \rangle = 0$, in which case the equation that we discretize is equivalent to

$$\partial_t^2 h^\epsilon + \epsilon \Lambda^s h_t^\epsilon = Ag\Lambda h^\epsilon - \frac{\sigma}{\rho^+ + \rho^-}\Lambda^3 h^\epsilon - A\partial_\alpha (H h_t^\epsilon h_t^\epsilon)\,. \tag{63$'$}$$

For $N = 0, 1, 2, \ldots$, we define the Fourier approximation using our projection operator P_N (introduced in section 7), defined as

$$P_N f(\alpha) = \sum_{-N}^{N} \hat{f}(k) e^{ik\alpha}\,.$$

Hence, the mesh size of our algorithm is given by

$$dx = \frac{2\pi}{N}\,.$$

We make use of the following identities in frequency space:

$$\begin{aligned}
\widehat{\partial_\alpha^n f}(k) &= (ik)^n \hat{f}(k)\,,\\
\widehat{Hf}(k) &= -i\mathrm{sgn}(k)\hat{f}(k)\,,\\
\widehat{\Lambda f}(k) &= -i\mathrm{sgn}(k) ik \hat{f}(k) = |k|\hat{f}(k)\,,\\
\widehat{fg}(k) &= \hat{f} * \hat{g}(k)\,.
\end{aligned}$$

It follows that in frequency space, the system (62) can be written as

$$\begin{aligned}
\frac{d}{dt}\hat{h}^\epsilon &= \frac{-i\mathrm{sgn}(k)}{2}\hat{\varpi}^\epsilon\,,\\
\frac{d}{dt}\hat{\varpi}^\epsilon &= 2Agik\hat{h}^\epsilon + \frac{2\sigma}{\rho^+ + \rho^-}(ik)^3\hat{h}^\epsilon - \langle \varpi_0 \rangle ik \left(\frac{\varpi^\epsilon}{4\pi}(-k^2\hat{h}^\epsilon)\check{}\right)\hat{}\\
&\quad + \frac{A}{4\pi}ik|k|\hat{\varpi}^\epsilon\langle\varpi_0\rangle - \frac{A}{2}|k|\left(\varpi^\epsilon\left(-i\mathrm{sgn}(k)\hat{\varpi}^\epsilon\right)\check{}\right)\hat{} - \epsilon|k|^3\hat{\varpi}^\epsilon\,.
\end{aligned}$$

This is a nonlinear system of ordinary differential equations, to which we shall apply the adaptive Runge–Kutta–Fehlberg fourth-order (nominally fifth-order) scheme to advance in time increments.

For the following simulations, we have set the acceleration to a constant value of g, which will either act downward or upward, depending on the type of RT instability that we examine. The initial position of the interface is specified, as well as the initial amplitude of the vorticity, $\varpi(\alpha, 0)$.

9.1.2. Numerical approximation of the z-model. We change variables and consider that the curve $z(\alpha, t)$ is given by

$$z(\alpha, t) = (\alpha + \delta z_1(\alpha, t), z_2(\alpha, t)),$$

where $\delta z_1, z_2$ are periodic functions defined on $[-\pi, \pi]$.

For our numerical simulations, we shall only consider the case of zero surface tension. We use the same Fourier-collocation method described previously (with N

Fourier modes) to approximate the following system of equations:

$$(\delta z_1)^\epsilon_t = -\frac{1}{2} H \varpi^\epsilon \frac{\partial_\alpha z_2^\epsilon}{|(1+\partial_\alpha \delta z_1^\epsilon, \partial_\alpha z_2^\epsilon)|^2} + \epsilon \partial_\alpha^2 \delta z_1^\epsilon \,, \tag{64a}$$

$$(z_2)^\epsilon_t = \frac{1}{2} H \varpi^\epsilon \frac{1+\partial_\alpha \delta z_1^\epsilon}{|(1+\partial_\alpha \delta z_1^\epsilon, \partial_\alpha z_2^\epsilon)|^2} + \epsilon \partial_\alpha^2 z_2^\epsilon \,, \tag{64b}$$

$$\varpi^\epsilon_t = -\partial_\alpha \left[\frac{A}{2} \frac{1}{|(1+\partial_\alpha \delta z_1^\epsilon, \partial_\alpha z_2^\epsilon)|^2} H\left(\varpi^\epsilon H \varpi^\epsilon\right) - 2Ag z_2^\epsilon \right] + \epsilon \partial_\alpha^2 \varpi^\epsilon \,. \tag{64c}$$

The system (64) employs an artificial viscosity term $\epsilon \partial_\alpha^2$ to stabilize small-scale noise.

9.2. Simulation 1: h-model, $\frac{\rho^+}{\rho^-} = \frac{1}{1.5}$ and Atwood number $A < 0$. We first study the effect of the density ratio on the interface motion given by the simple RT h-model (62) in the absence of surface tension ($\sigma = 0$). For our first simulation, we consider two fluids with density ratio 1/1.5.

Specifically, we consider the physical parameters set to

$$g = 9.8 \text{ m/s},\ \sigma = 0,\ \rho^+ = 1 \text{ kg/m}^3,\ \rho^- = 1.5 \text{ kg/m}^3,\ \text{so } A = -0.2\,,$$

with initial data

$$h(\alpha, 0) = \sin(3\alpha)\,, \tag{65}$$

$$\varpi(\alpha, 0) = 2H \sin(2\alpha)\,. \tag{66}$$

In order to study convergence of our scheme and the effect of the artificial viscosity operator, we perform a number of different simulations, varying the total number of modes N that are used, as well as the power on the artificial viscosity operator s and the size of the artificial viscosity parameter ϵ. In particular, we consider the following cases:

- $N = 2^7$, $\epsilon = 0.01$, $s = 3$ (red solid line in Figures 2 and 3);
- $N = 2^7$, $\epsilon = 0.008$, $s = 3$ (blue solid line with + markers in Figures 2 and 3);
- $N = 2^8$, $\epsilon = 0.008$, $s = 3$ (green dashed line in Figures 2 and 3);
- $N = 2^7$, $\epsilon = 0.04$, $s = 2$ (black dash-dot line in Figures 2 and 3).

The results are shown in Figures 2 and 3.

Note that the results are qualitatively similar for various values of parameters and, in particular, show the convergence of the numerical solutions with mesh size N. A comparison of the blue and the green curves in Figures 2 and 3 demonstrates this nicely.

Furthermore, as shown in Figure 2, there is a large jump in the amplitude of the interface $\|h\|_{L^\infty}$ over a very small time scale. Specifically, we see that for an $O(1)$ initial interface position and velocity, the amplitude of the interface, $\|h\|_{L^\infty}$, grows by a factor of 4 in a time 0.45. See Figure 3 for the comparison of the interface position $h(x, t_1)$ at time $t_1 = 1.95$ and interface position $h(x, t_2)$ at time $t_2 = 2.4$.

9.3. Simulation 2: h-model, $\frac{\rho^+}{\rho^-} = \frac{1.23}{1027}$ for Atwood number $A < 0$. Next, we consider the physical parameters

$$g = 9.8 \text{ m/s},\ \sigma = 0,\ \rho^+ = 1.23 \text{ kg/m}^3,\ \rho^- = 1027 \text{ kg/m}^3,\ \text{so } A = -0.99761.$$

This corresponds to the density of air (ρ^+) and ocean water (ρ^-).

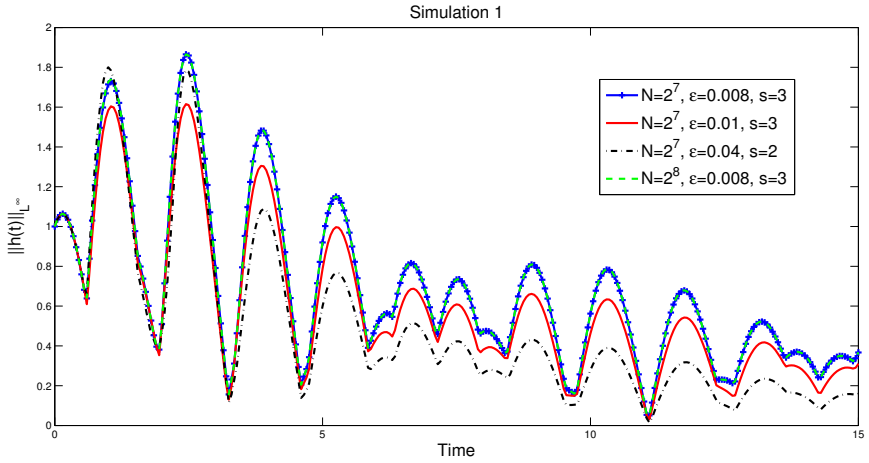

FIG. 2. *Evolution of the maximum amplitude of* $|h(x,t)|$*, written as* $\|h(t)\|_{L^\infty}$.

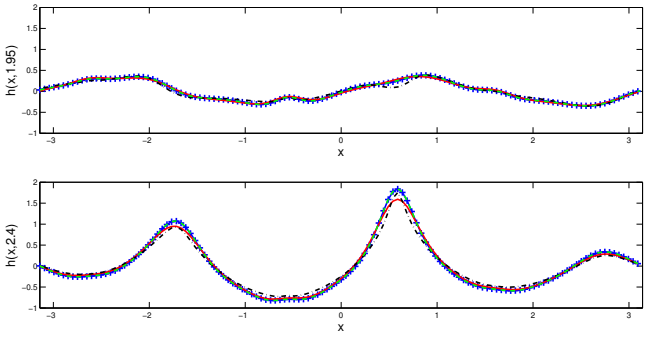

FIG. 3. *Interface position* $h(x,t_j)$ *for* $t_1 = 1.95$ *and* $t_2 = 2.4$.

We consider the initial data (65) and (66) for (62). The artificial viscosity $\epsilon = 0.05$ and the order of the artificial viscosity operator is $s = 3$. The number of nodes is $N = 2^7$. The results of this simulation are shown in Figure 4, wherein, we once again see the fast growth of the interface $\|h(t)\|_{L^\infty}$ over a short time scale, followed by decay to equilibrium. The heavier fluid in this simulation, as compared to Simulation 1, reduces the frequency of oscillations, as the interface decays to the rest state. From the intial data, the amplitude grows from 0.7 to 4.3 in a time scale of length 0.2 (between $t = 0.2$ and $t = 0.4$). After this remarkable growth, the amplitude of the interface decays and approaches the rest state (see the blue curve in Figure 4). In order to demonstrate the role of the nonlinearity in the growth of the interface, we compare this to the linear h-model (17). As expected, the linear model simply decays the interface amplitude; see the red curve in Figure 4.

Finally, in Figure 5 we plot the energy spectrum

$$\mathcal{E}(k,t) = |\hat{h}_t(k,t)|^2 - Ag|k||\hat{h}(k,t)|^2,$$

associated with the energy law (39a) in Proposition 7.3, as a function of k at $t_0 = 0, t_1 = 0.2, t_2 = 0.45$, and $t_3 = 0.7$. We note that outside the Fourier modes $k \in$

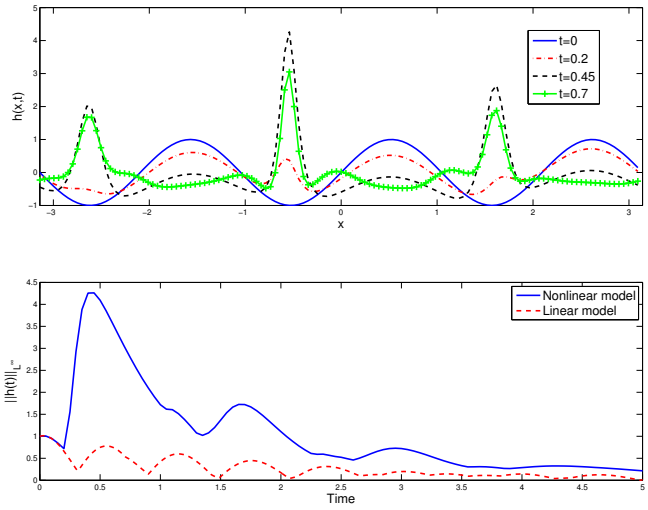

FIG. 4. (a) *Interface position* $h(x,t_j)$ *for* $t_1 = 0$, $t_2 = 0.2$, $t_3 = 0.45$, *and* $t_4 = 0.7$. (b) $\|h(t)\|_{L^\infty}$ *as a function of time.*

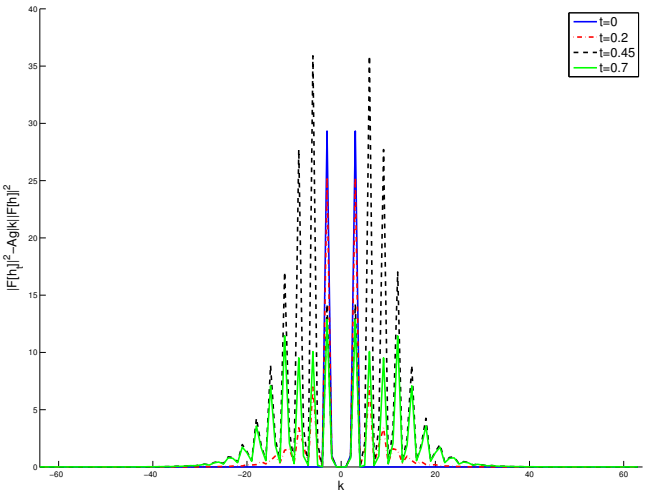

FIG. 5. *The energy spectrum* $|\hat{h}_t(k,t)|^2 - Ag|k||\hat{h}(k,t)|^2$ *as a function of the Fourier mode* k *at* $t_0 = 0, t_1 = 0.2, t_2 = 0.45$, *and* $t_3 = 0.7$.

$[-50, 50]$, the energy spectrum $\mathcal{E}(k,t)$ is of order 10^{-4} for the time interval considered. Starting from a mode-3 initial interface shape, the energy content is distributed into the smaller scales. At time $t = .45$ when the interface is of maximum amplitude, the energy content is well-distributed among all large scales $|k| \leq 20$.

9.4. Simulation 3: *h*-model, fingering instability, Atwood number $A > 0$. We next simulate the highly unstable case of a heavy fluid on top of the lighter fluid, and with the acceleration acting downward. We consider the following physical parameters:

$$g = 9.8 \text{ m/s},\ \sigma = 0,\ \rho^+ = 10 \text{ kg/m}^3,\ \rho^- = 1 \text{ kg/m}^3,\ \text{so } A = 0.81818\,.$$

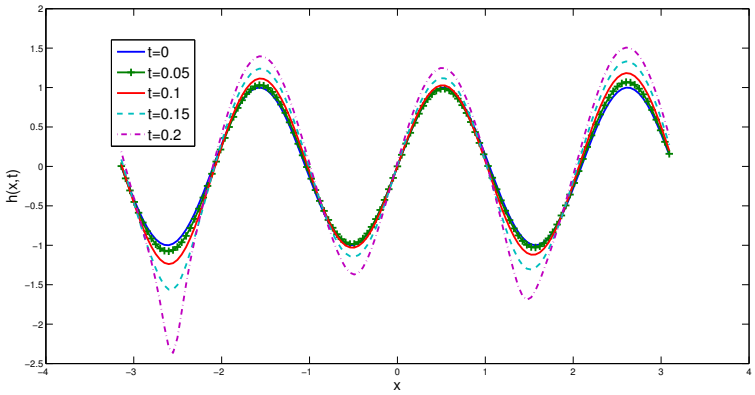

FIG. 6. *Interface position* $h(x,t_j)$ *for* $t_1 = 0$, $t_2 = 0.05$, $t_3 = 0.1$, $t_4 = 0.15$, *and* $t_5 = 0.2$.

We once again use our order one initial data (65) and (66) for (62). The artificial viscosity operator is order $s = 3$, and the artificial viscosity parameter is set to $\epsilon = 0.05$. The number of nodes is $N = 2^7$.

This simulation is intended to demonstrate the ability of the h-model to show fingering phenomenon; indeed, as can be seen in Figure 6, the heavy fluid penetrates the lighter fluid and a strong RT instability is initiated. After a large enough time interval, the absolute value of the interface grows exponentially fast.

9.5. Simulation 4: *h*-model, stability, Atwood number $A < 0$. To capture the behavior described in Theorem 7.6, we simulate (63′) (instead of (62)). We consider the physical parameters

$$g = 9.8 \text{ m/s},\ \sigma = 0,\ \rho^+ = 0 \text{ kg/m}^3,\ \rho^- = 1 \text{ kg/m}^3,\ \text{so } A = -1\,,$$

and the initial data

$$h_0 = \frac{\cos(\alpha)}{10},\ h_1 = -1 + \frac{\sin(\alpha)}{10}.$$

For these initial data, the homogeneous solution $h^\infty(t)$ is given by

$$h^\infty(t) = -t.$$

Theorem 7.6 states that $h(\cdot,t) - h^\infty(t)$ converges to zero as $t \to \infty$.

As the initial data satisfy the stability condition, no artificial viscosity is required to stabilize the numerical solution, and we set $\epsilon = 0$. Finally, we fix the number of Fourier modes to $N = 2^7$. The results are plotted in Figure 7, where the simulation demonstrates the asymptotic behavior of the theorem.

9.6. Simulation 5: The rocket rig experiment of Read and Youngs. We consider now the situation where two (nearly) incompressible fluids, of densities $\rho^\pm$, are subjected to an approximately constant acceleration g normal to the interface separating them, directed from the lighter fluid to the denser fluid. We assume that the initial interface is given by a *small and random* perturbation of the flat state.

Our goal is to compare the growth rate of the mixing layer using our model (24) with that predicted by experiments and numerical simulations of Read [13] and Youngs [19]. Experiments show that if the instability arises in the previous setting, the width of the mixed region grows like t^2. Actually, as shown by Read [13] and

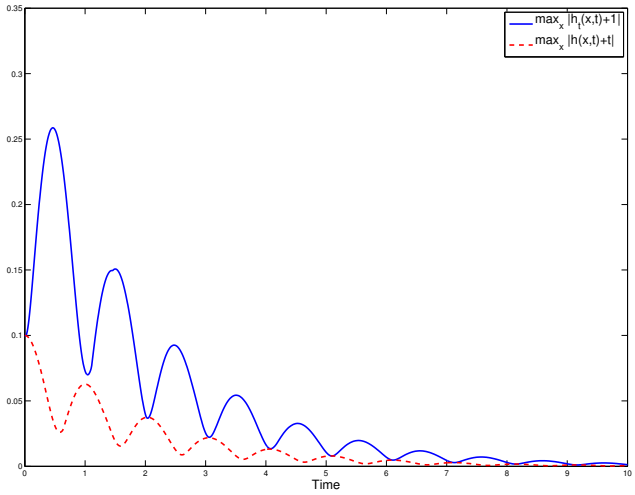

FIG. 7. *Distance from $h(x,t)$ to $h^\infty(t)$ (dashed line) and from $h_t(x,t)$ to -1.*

Youngs [19], the mixing region grows as

$$\delta A g t^2. \tag{67}$$

DNS in two space dimensions by Youngs [19] has indicated that the parameter δ should range from 0.04 to 0.05, whereas experiments of Read [13] suggest that δ should range from 0.06 to 0.07. In particular, when we have a NaI solution ($\rho^- = 1.89$ g/cm^3) and hexane ($\rho^+ = 0.66$ g/cm^3) in a tank, the empirical value is $\delta = 0.063$ (see [13]). Let us emphasize that both the numerical simulations and the physical experiments were run for approximately 70 ms.

9.6.1. The *h*-model. We consider the initial data for the h-model, given by

$$h(\alpha,0) = S\sum_{j=1}^{n} a_j \cos(jx) + b_j \sin(jx), \tag{68}$$

$$\varpi(\alpha,0) = 0, \tag{69}$$

where a_j, b_j are random numbers following a standard Gaussian distribution, and S denotes a normalization constant such that

$$\|h(0)\|_{L^2} = \frac{\pi}{100}.$$

We consider $n = 50$, $N = 2^7$, and $\sigma = 0$.

The acceleration $g = -\frac{9.8\cdot 2\cdot \pi}{0.3} L/s^2$ acts upwards, where L is chosen so that $2\pi/0.3\, L = 1$ m. This gravity force corresponds to the usual gravity force on the surface of the Earth of 9.8 m/s^2. Finally, we use the artificial viscosity parameter $\epsilon = 0.05$ together with a second-order artificial viscosity operator $s = 2$.

The mixing layer is shown in Figure 8, where the interface position $h(x,t_j)$ is displayed for times $t_1 = 0$, $t_2 = 0.02$, $t_3 = 0.04$, $t_4 = 0.06$, and $t_5 = 0.08$.

In Figure 9, we see that up to time $t = 150$ ms, the numerical solution provides a mixing layer growth rate which agrees well with the predicted growth rate given by

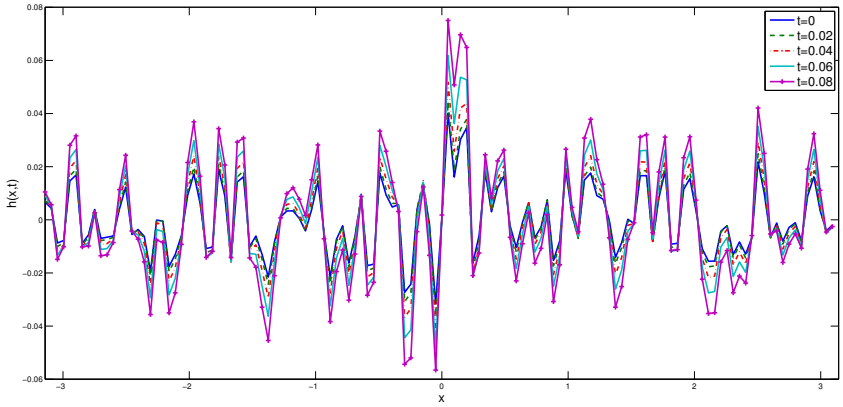

FIG. 8. *Interface position* $h(x,t_i)$ *for* $t_1 = 0$, $t_2 = 0.02$, $t_3 = 0.04$, $t_4 = 0.06$, *and* $t_5 = 0.08$.

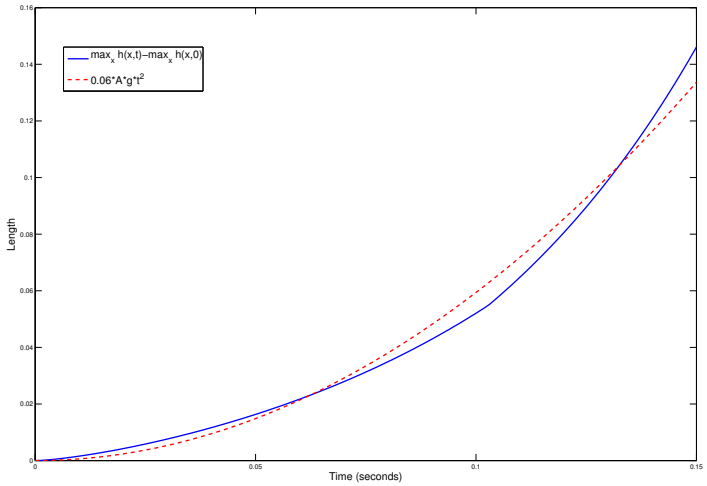

FIG. 9. *Comparison between* $\max_x h(x,t) - \max_x h(x,0)$ *and the predicted quadratic growth rate* (67) *with* $\delta = 0.06$.

(67); the largest difference between the h-model and (67) is given by

$$\max_{0\le t\le 150ms} \max_x h(x,t) - \max_x h(x,0) - 0.06Agt^2 = 0.002916\,.$$

For large times, due to the strong RT instability present in the equations, the results of numerical simulations are very sensitive to the artificial viscosity parameter (see [7] for the artificial viscosity effects on RT mixing rates); however, for short time (meaning around 70 ms, neither viscosity nor nonlinearity plays a critical role in the evolution. To demonstrate this, we perform a numerical simulation of the h-model with zero artificial viscosity $\epsilon = 0$, and with surface tension $\sigma = 0.005$. We use the initial data satisfying (68)–(69) with $n = 30$, and S chosen such that

$$\|h(0)\|_{L^2} = \frac{\pi}{1000}.$$

As can be seen in Figure 10, the growth rate predicted by our model agrees well with the Youngs' growth rate with $\delta = 0.06$ up to around $t = 60$ ms.

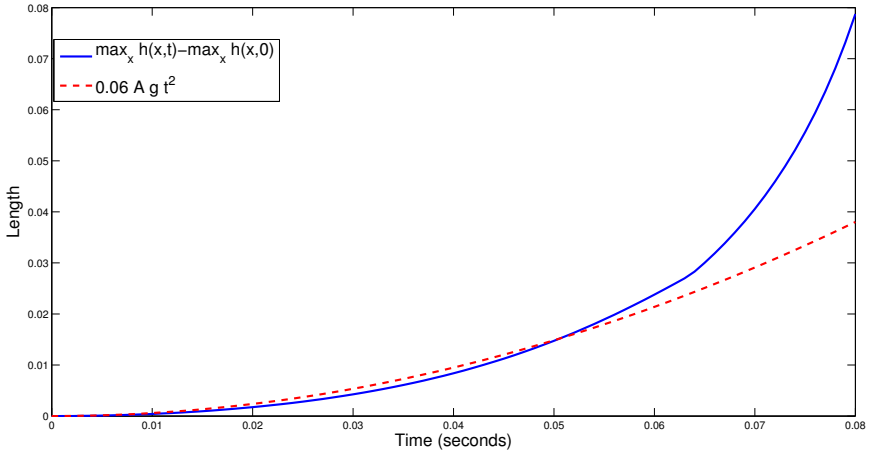

FIG. 10. *Comparison between* $\max_x h(x,t) - \max_x h(x,0)$ *and* (67) *(with* $\delta = 0.06$*) without artificial viscosity.*

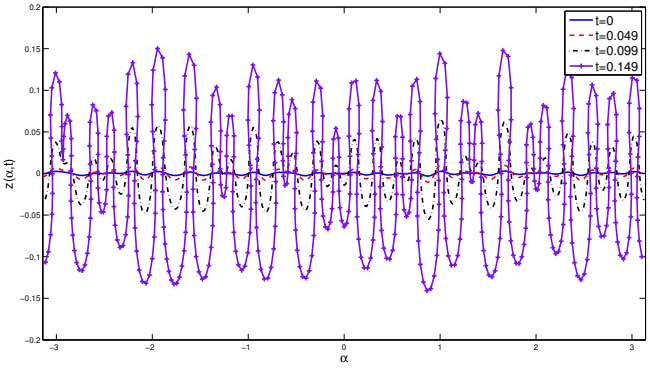

FIG. 11. *Interface position* $z(\alpha, t_j)$ *for* $t_0 = 0$, $t_1 = 0.049$, $t_2 = 0.099$, *and* $t_3 = 0.149$.

9.6.2. The *z*-model. Now, we repeat the rocket rig experiment of Read and Youngs using the z-model, with initial data given by

$$\delta z_1(\alpha, 0) = 0, \tag{70}$$

$$z_2(\alpha, 0) = S \sum_{j=1}^{n} a_j \cos(jx) + b_j \sin(jx), \tag{71}$$

$$\varpi(\alpha, 0) = 0, \tag{72}$$

where a_j, b_j are random numbers following a standard Gaussian distribution, and S denotes a normalization constant such that

$$\|z_2(0)\|_{L^2} = \frac{\pi}{1000}.$$

We consider $n = 30$ and $N = 2^9$. The artificial viscosity for (64) has coefficient $\epsilon = 0.01$. Figure 11 shows the interface evolution for the z-model. The ability of the z-model parameterization to "fatten" and "finger" produces an even more accurate representation of the mixing region.

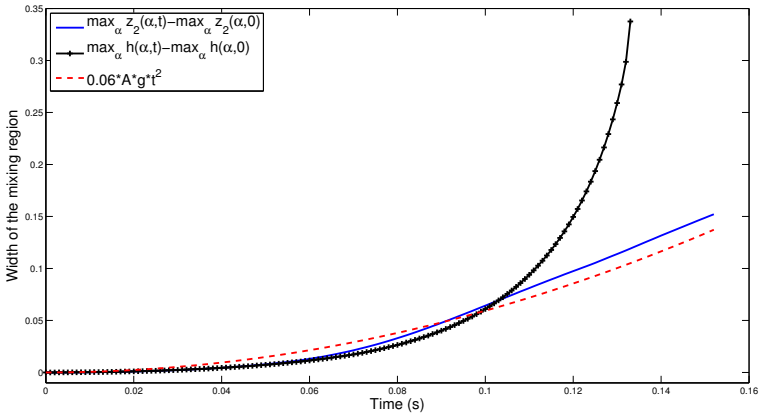

FIG. 12. *Comparison between* $\max_x z_2(x,t) - \max_x z_2(x,0)$, $\max_x h(x,t) - \max_x h(x,0)$, *and* (67) *with* $\delta = 0.06$.

We are able to quantitatively validate this statement by comparing the growth of the mixing region of the z-model with the h-model and the quadratic prediction (67) of Read and Youngs. For the comparison, we simulate the h-model with the same physical parameters, and with second-order artificial viscosity with $\epsilon = 0.05$, and with initial data given by

$$h(\alpha,0) = z_2,$$
$$\varpi(\alpha,0) = 0.$$

We note that the artificial viscosity ϵ is five times larger for the h-model (62) than for the z-model (64). As shown in Figure 12, the z-model mixing region growth rate matches very well with the quadratic prediction (67) of Read and Youngs, and for a relatively long time interval, up to $t = 150$ ms. The width of the mixing region, approximated by

$$\max_\alpha z_2(\alpha,t) - \max_\alpha z_2(\alpha,0)\,,$$

is in excellent agreement with the quadratic prediction (67). The maximum error for the z-model is

$$\max_{0\le t\le 0.152} \left| \max_\alpha z_2(\alpha,t) - \max_\alpha z_2(\alpha,0) - 0.06Agt^2 \right| \approx 0.01537\,,$$

whereas the maximum error for the h-model is

$$\max_{0\le t\le 0.133} \left| \max_\alpha h(\alpha,t) - \max_\alpha h(\alpha,0) - 0.06Agt^2 \right| \approx 0.23244\,.$$

Moreover, the z-model has a longer lifespan than the h-model. Since the h-model is constrained to remain a graph, the amplitude of the interface can only grow rapidly once the RT instability is strongly initiated; on the other hand, as the z-model can turn over, the instability creates a turnover and horizontal fattening of the mixing region. The comparison is shown in Figure 13.

9.7. Simulation 6: The tilted rig experiment. Finally, we consider the "tilted" rig experiment of Youngs [19], wherein the tank of the rocket rig experiment is titled by a small angle θ from the vertical.

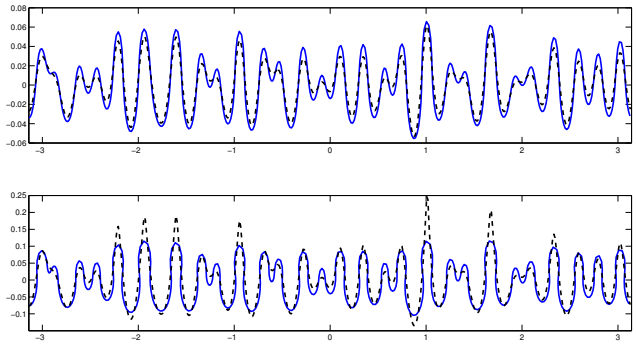

FIG. 13. *Comparison between $h(\alpha, t_j)$ (dashed line) and $z(\alpha, t_j)$ (solid line) at $t_1 = 0.099$ and $t_2 = 0.129$.*

Again, we have two (nearly) incompressible fluids, of densities $\rho^{\pm}$, with a vertical acceleration g directed from the lighter fluid to the denser fluid. As Youngs notes, the inclination of the initial interface results in a gross overturning motion in addition to the fine-scale mixing.

We define $\theta = 5.7^\circ$ and consider the unperturbed (flat) *tilted* interface given by

$$\tilde{z}_0^2 = \begin{cases} \tan(\theta)(x+\pi) & \text{if } -\pi \le x < -\pi/2, \\ -\tan(\theta)x & \text{if } |x| \le \pi/2, \\ \tan(\theta)(x-\pi) & \text{if } \pi/2 < \pi \le \pi. \end{cases}$$

We assume that the actual initial interface is given by a *small and random* perturbation so that

$$z_0^2(x) = \tilde{z}_0^2(x) + S \sum_{j=1}^{n} a_j \cos(jx) + b_j \sin(jx),$$

where a_j, b_j are random numbers following a standard Gaussian distribution, and S denotes a normalization constant such that

$$\|z_0^2 - \tilde{z}_0^2\|_{L^2} = \frac{\pi}{1000}.$$

We fix $n = 30$ and $N = 2^9$.

9.7.1. The *h*-model. The initial data for the h-model (62) are given by

$$h(\alpha, 0) = z_0^2(\alpha)\,, \tag{73}$$

$$\varpi(\alpha, 0) = 0\,. \tag{74}$$

Again, we employ a second-order artificial viscosity operator with $\epsilon = 0.25$, a rather large artificial viscosity, but necessary to stabilize the interface in the highly unstable RT regime. The results are plotted in Figure 14.

9.7.2. The *z*-model. For the z-model, we use the initial conditions

$$\delta z_1(\alpha, 0) = 0\,,\ z_2(\alpha, 0) = z_0^2(\alpha)\,,\ \varpi(\alpha, 0) = 0$$

with artificial viscosity $\epsilon = 0.05$. As can be seen in Figure 14, as the RT instability is strongly initiated, the amplitude of the h-model starts to grow unboundedly, while the z-model can turn over and continue to run for a much longer time interval.

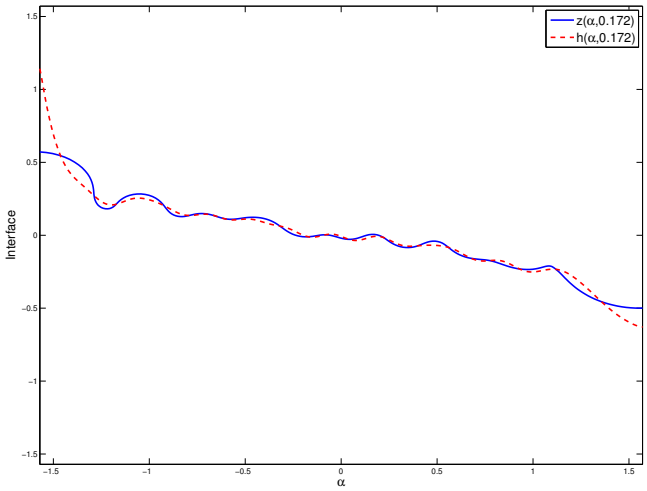

FIG. 14. *Interface position* $h(\alpha, t_j)$ *(dashed line) and* $z(\alpha, t_j)$ *(solid line) for* $t = 0.172$.

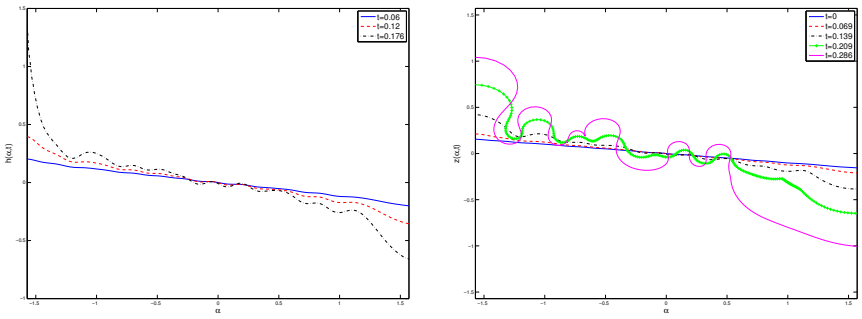

(a) h-model (b) z-model

FIG. 15. *Interface position for* $t_0 = 0$, $t_1 = 0.069, t_2 = 0.139, t_3 = 0.209$, *and* $t_4 = 0.286$.

We show the time evolution of the interface for the h-model and z-model in Figure 15. Because the h-model can only grow the amplitude of h, the behavior of the interface is more singular for the h-model than for the z-model. In particular, $\|h(t)\|_{L^\infty}$ grows faster than $\|z_2(t)\|_{L^\infty}$. Moreover, the z-model is more stable, and permits the use of smaller artificial viscosity than the h-model.

Finally, as we have run the titled rig experiment with random initial data, it is interesting to plot the ensemble of runs, and get a clear picture of the mixing region. In particular, as it may be difficult to infer the qualitative description of the mixing region from only one simulation, in Figure 16, we plot the z-model interface location for a number of different random initial conditions at time $t = 0.22$. As can be seen, the ensemble gives an approximation of the mixing region provided by experiment [19] and DNS [15]. The mixing region grows slightly faster on the left side than it drops on the right side as expected by Youngs [19], and has the qualitative features of the experiment.

9.8. Simulation 7: z-model, Kelvin–Helmholtz instability, Atwood number $A = 0$. The z-model can simulate the Kelvin–Helmholtz instability arising in

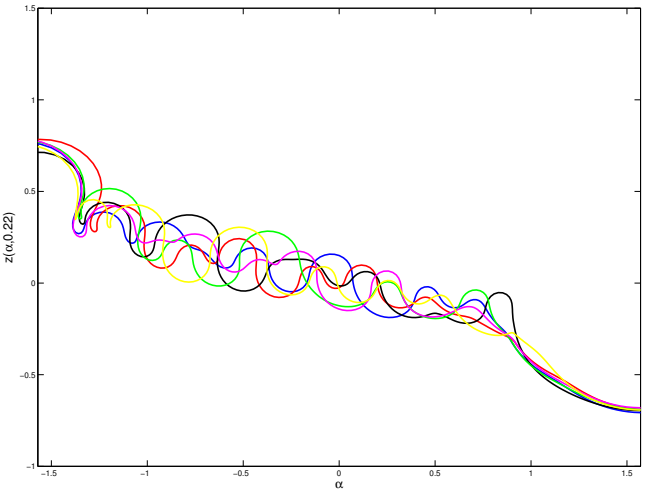

FIG. 16. *An ensemble of z-model interface positions for* $t = 0.22$.

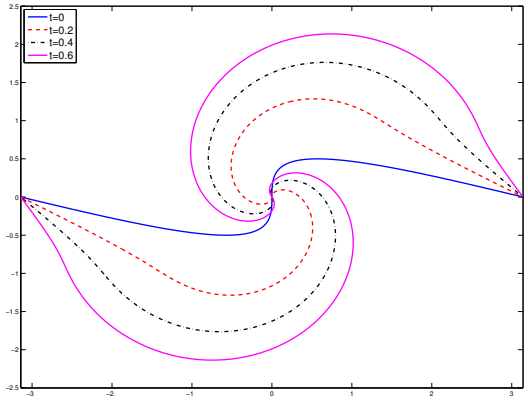

FIG. 17. *The interface* $z(\alpha, t)$ *at* $t_0 = 0, t_1 = 0.2, t_2 = 0.4$, *and* $t_3 = 0.6$.

the case of equal densities $\rho^+ = \rho^-$, equivalently $A = 0$. We note that when $A = 0$, due to (59), we have

$$\varpi_t = 0,$$

and the problem reduces to describing the interface evolution for $z(\alpha, t)$ via (64a), (64b). We consider the initial data given by

$$\delta z_1(\alpha, 0) = -\sin(\alpha)\,, \;\; z_2(\alpha, 0) = 0.5\sin(\alpha)\,,$$

and

$$\varpi(\alpha) = 10\cos(\alpha)\,,$$

and use $N = 2^8$ Fourier modes. We fix the artificial viscosity as $\epsilon = 0.01$. The results are given in Figure 17. The primary effect of the nonlinearity is to increase the length of the interface by starting to roll over, while keeping the curve smooth.

This can be seen by looking at the spectral content of the the L^2-energy function

$$\mathcal{E}(k, t) = |\delta\hat{z}_1(k, t)|^2 + |\hat{z}_2(k, t)|^2$$

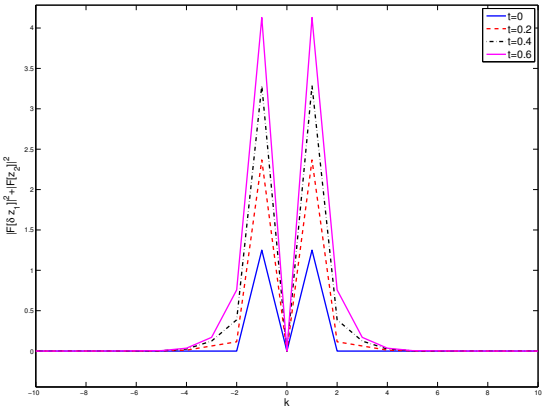

FIG. 18. *The energy spectrum* $|\delta\hat{z}_1(k,t)|^2 + |\hat{z}_2(k,t)|^2$ *as a function of the Fourier mode* $k \in [-10, 10]$ *at* $t_0 = 0, t_1 = 0.2, t_2 = 0.4$, *and* $t_3 = 0.6$.

at different instances of time. In Figure 18 we plot the spectrum of $\mathcal{E}(k,t)$ at times $t_0 = 0, t_1 = 0.2, t_2 = 0.4$, and $t_3 = 0.6$. For large Fourier modes $|k| > 10$, the L^2-energy spectrum $\mathcal{E}(k,t)$ is of order 10^{-5} for the time interval considered, so we plot $\mathcal{E}(k,t)$ versus $-10 \leq k \leq 10$. The energy spectrum remains fairly localized about the $k = 1$ initial data, with some growth in wavenumbers $|k| = 2$ and 3, which are responsible for the dilation and rotation of the wave.

REFERENCES

[1] H. Bae, and R. Granero-Belinchón, *Global existence for some transport equations with nonlocal velocity*, Adv. Math. 269 (2015), pp. 197–219.

[2] L. Caffarelli and J.L. Vázquez, *Nonlinear porous medium flow with fractional potential pressure*, Arch. Ration. Mech. Anal., 202 (2011), pp. 537–565.

[3] J.A. Carrillo, L.C.F. Ferreira, and J.C. Precioso, *A mass-transportation approach to a one dimensional fluid mechanics model with nonlocal velocity*, Adv. Math., 231 (2012), pp. 306–327.

[4] A. Castro and D. Córdoba, *Global existence, singularities and ill-posedness for a nonlocal flux*, Adv. Math., 219 (2008), pp. 1916–1936.

[5] D. Chae, A. Cordoba, D. Cordoba, and M. Fontelos, *Finite time singularities in a 1D model of the quasi-geostrophic equation*, Adv. Math., 194 (2005), pp. 203–223.

[6] A. Córdoba, D. Córdoba, and F. Gancedo, *Interface evolution: Water waves in 2-D*. Adv. Math., 223 (2010), pp. 120–173.

[7] J. Glimm, J.W. Grove, X.L. Li, W. Oh, and D.H. Sharp, *A critical analysis of Rayleigh-Taylor growth rates*, J. Comput. Phys., 169 (2001), pp. 652–677.

[8] V.N. Goncharov, *Analytical model of nonlinear, single-mode, classical Rayleigh-Taylor instability at arbitrary Atwood numbers*, Phys. Rev. Lett., 88 (2002), 134502.

[9] A. Ilyin, A. Laptev, M. Loss, and S. Zelik, *One-dimensional interpolation inequalities, Carlson–Landau inequalities, and magnetic Schrödinger operators*, Int. Math. Res. Not. IMRN, 2016 (2015), pp. 1190–1222.

[10] C.E. Kenig, G. Ponce, and L. Vega, *Well-posedness and scattering results for the generalized Korteweg-de-Vries equation via the contraction principle*, Comm. Pure App. Math, 46 (1993), pp. 527–620.

[11] H.J. Kull, *Theory of the Rayleigh-Taylor instability*, Phys. Rep., 206 (1991), pp. 197–325.

[12] L. Rayleigh, *On the instability of jets*, Proc. London Math. Soc. (1), 10 (1878), pp. 4–13.

[13] K.I. Read, *Experimental investigation of turbulent mixing by Rayleigh-Taylor instability*, Phys. D, 12 (1984), pp. 45–58.

[14] J. Reisner, J. Serencsa, and S. Shkoller, *A space-time smooth artificial viscosity method for nonlinear conservation laws*, J. Comput. Phys., 235 (2013), pp. 912–933.

[15] B. Rollin and M.J. Andrews, *On generating initial conditions for turbulence models: The case of Rayleigh-Taylor instability turbulent mixing*, J. Turbul., 14 (2013), pp. 77–106.
[16] D.H. Sharp, *An overview of Rayleigh-Taylor instability*, Phys. D, 12 (1984), pp. 3–18.
[17] G. Taylor, *The instability of liquid surfaces when accelerated in a direction perpendicular to their planes.* 1, R. Soc. Lond. Proc. Ser. A. Math. Phys. Eng. Sci., 201 (1950), pp. 192–196.
[18] D.L. Youngs, *Numerical-simularion of turbulent mixing by Rayleigh-Taylor instability*, Phys. D, 12 (1984), pp. 32–44.
[19] D.L. Youngs, *Modeling turbulent mixing by Rayleigh-Taylor instability*, Phys. D, 37 (1989), pp. 270–287.